Monthly Notices
of the
ROYAL ASTRONOMICAL SOCIETY

Mon. Not. R. Astron. Soc. **401,** 2181–2201 (2010) doi:10.1111/j.1365-2966.2009.15819.x

Simulations of quintessential cold dark matter: beyond the cosmological constant

E. Jennings,[1,2]★ C. M. Baugh,[1] R. E. Angulo[3] and S. Pascoli[2]

[1]*Institute for Computational Cosmology, Department of Physics, University of Durham, South Road, Durham DH1 3LE*
[2]*Institute for Particle Physics Phenomenology, Department of Physics, University of Durham, South Road, Durham DH1 3LE*
[3]*Max Planck Institute fur Astrophysik, D-85741 Garching, Germany*

Accepted 2009 October 2. Received 2009 October 1; in original form 2009 August 7

ABSTRACT

We study the non-linear growth of cosmic structure in different dark energy models, using large volume *N*-body simulations. We consider a range of quintessence models which feature both rapidly and slowly varying dark energy equations of state, and compare the growth of structure to that in a universe with a cosmological constant. We use a four-parameter equation of state for the dark energy which accurately reproduces the quintessence dynamics over a wide range of redshifts. The adoption of a quintessence model changes the expansion history of the universe, the form of the linear theory power spectrum and can alter key observables, such as the horizon scale and the distance to last scattering. We incorporate these effects into our simulations in stages to isolate the impact of each on the growth of structure. The difference in structure formation can be explained to first order by the difference in growth factor at a given epoch; this scaling also accounts for the non-linear growth at the 15 per cent level. We find that quintessence models that are different from Λ cold dark matter (ΛCDM) both today and at high redshifts ($z \sim 1000$), and which feature late ($z < 2$), rapid transitions in the equation of state, can have identical baryonic acoustic oscillation (BAO) peak positions to those in ΛCDM. We find that these models have higher abundances of dark matter haloes at $z > 0$ compared to ΛCDM and so measurements of the mass function should allow us to distinguish these quintessence models from a cosmological constant. However, we find that a second class of quintessence models, whose equation of state makes an early ($z > 2$) rapid transition to $w = -1$, cannot be distinguished from ΛCDM using measurements of the mass function or the BAO, even if these models have non-negligible amounts of dark energy at early times.

Key words: methods: *N*-body simulations – cosmology: theory – large-scale structure of Universe.

1 INTRODUCTION

Determining whether or not the dark energy responsible for the accelerating expansion of the Universe evolves with time remains a key goal of physical cosmology. This will tell us if the dark energy is indeed a cosmological constant or has a dynamical form as in quintessence models. The nature of the dark energy determines the expansion history of the Universe and hence the rate at which cosmological perturbations grow. In this paper, we investigate the influence of quintessence dark energy on the non-linear stages of structure formation using a suite of *N*-body simulations.

The simplest candidate for dark energy is the cosmological constant, Λ (see e.g. the review by Carroll 2001). Despite the success of ΛCDM (cold dark matter and cosmological constant model) at fitting much of the available observational data (Sanchez et al. 2009), this model fails to address two important issues: the fine-tuning problem and the coincidence problem. The fine-tuning problem arises from the vast discrepancy between the vacuum energy level predicted by particle physics, generically given by Λ^4, where Λ is the physics scale considered, and the value of missing energy density inferred cosmologically, $\rho \sim 10^{-47}\,\mathrm{GeV}^4$. In the standard model of particle physics, Λ could be at the Planck scale, $\Lambda \sim 10^{18}$ GeV. The coincidence problem refers to the fact that we happen to live around the time at which dark energy has emerged as the dominant component of the Universe, and has a comparable energy density to matter, $\rho_{\mathrm{DE}} \sim \rho_m$.

★E-mail: elise.jennings@durham.ac.uk

Quintessence models were devised to solve the fine-tuning and coincidence problems of ΛCDM. In these models, the cosmological constant is replaced by an extremely light scalar field which evolves slowly (Ratra & Peebles 1988; Wetterich 1988; Caldwell, Dave & Steinhardt 1998; Ferreira & Joyce 1998). An abundance of quintessence models has been proposed in the literature which can resolve the coincidence problem and explain the observationally inferred amount of dark energy. Models of quintessence dark energy can have very different potentials, $V(\varphi)$, but can share common features. The potentials provide the correct magnitude of the energy density and are able to drive the accelerated expansion seen today. The form of the scalar field potential determines the trajectory of the equation of state, $w(z) = P/\rho$, as it evolves in time. Hence, different quintessence dark energy models have different dark energy densities as a function of time, $\Omega_{\rm DE}(z)$. This implies a different growth history for dark matter perturbations from that expected in ΛCDM.

Cosmological N-body simulations are the theorist's tool of choice for modelling the final stages of perturbation collapse. The overwhelming majority of simulations have used the concordance ΛCDM cosmology. Here we simulate different dark energy models and study their observational signatures. A small number of papers have used N-body simulations to test scalar field cosmologies (Ma et al. 1999; Linder & Jenkins 2003; Klypin et al. 2003; Francis, Lewis & Linder 2008; Alimi et al. 2009; Casarini, Macciò & Bonometto 2009; Grossi & Springel 2009). Rather than explicitly solving for different potentials, it is standard practice to modify the Friedmann equation using a form for the dark energy equation of state, $w(z)$. Previous work used a variety of parametrizations for $w(z)$, the most common being the two-parameter equation, $w = w_0 + (1 - a)w_a$ (Chevallier & Polarski 2001; Linder 2003) or the empirical three-parameter equation proposed by Wetterich (2004) for the so-called early dark energy models. The disadvantage of using a one- or two-variable parametrization for w is that it cannot accurately reproduce the dynamics of a quintessence model over a wide range of redshifts. If we wish to reproduce the equation of state of the original scalar field to within 5 per cent, a two-parameter equation of state will not be able to achieve this precision for a wide range of quintessence potentials (Bassett, Corasaniti & Kunz 2004). Instead, we take advantage of a parametrization for $w(z)$ which can describe a wide range of different models. In this work, we use a four-parameter dark energy equation of state which can accurately reproduce the original $w(z)$ for a variety of dark energy models to better than 5 per cent for redshifts $z < 10^3$ (Corasaniti & Copeland 2003).

In this paper, we present three stages of N-body simulations of structure formation in quintessence models. Each stage progressively relaxes the assumptions made and brings us closer to a full physical model. In the first stage, the initial conditions for each quintessence cosmology are generated using a ΛCDM linear theory power spectrum and the background cosmological parameters are the best-fitting values assuming a ΛCDM cosmology. The only departure from ΛCDM in this first stage is the dark energy equation of state and its impact on the expansion rate. In the second stage, we use a modified version of CAMB (Lewis & Bridle 2002) to generate a consistent linear theory power spectrum for each quintessence model. The linear theory power spectrum can differ from the power spectrum in ΛCDM due to the presence of non-negligible amounts of dark energy during the early stages of the matter-dominated era. This power spectrum is then used to generate the initial conditions for the N-body simulation which is again run for each dark energy model. The third and final stage in our analysis is to find the values for the cosmological parameters $\Omega_{\rm m}h^2$, $\Omega_{\rm b}h^2$ and H_0 (the matter density, baryon density and Hubble parameter, respectively) such that each model satisfies cosmological distance constraints. Recently, Alimi et al. (2009) used cosmic microwave background (CMB) and supernova (SN) data to constrain the parameters in the quintessence potential and the value of the matter density, $\Omega_{\rm m}h^2$, for two models. In this paper, we allow three parameters to vary when fitting each quintessence model to the available data. This distinction is important as changes in these parameters may produce compensating effects which result in the quintessence model looking like ΛCDM. For example, for a given dark energy equation of state, a lower value of the matter density may not result in large changes in the Hubble parameter if the value of H_0 is increased. In going through each of these stages, we build up a comprehensive picture of the quintessence models and their effect on the non-linear growth of structure.

This paper is organized as follows. In Section 2, we discuss quintessence models and the parametrization we use for the dark energy equation of state. We also outline the expected impact of different dark energy models on structure formation. In Section 3, we give the details of our N-body simulations. The main power spectrum results are presented in Section 4.3. Intermediate results are presented in Sections 4.1 and 4.2, which the reader may wish to omit on a first pass. In Section 4.4, we present the mass function predictions. In Section 4.5, we discuss the appearance of the baryonic acoustic oscillations (BAO) in the matter power spectrum. Finally, in Section 6, we present our conclusions.

2 QUINTESSENCE MODELS OF DARK ENERGY

Here we briefly review some general features of quintessence models; more detailed descriptions can be found, for example, in Ratra & Peebles (1988), Wetterich (1988), Ferreira & Joyce (1998), Copeland, Sami & Tsujikawa (2006) and Linder (2008). The main components of quintessence models are radiation, pressureless matter and a quintessence scalar field, denoted by φ. This dynamical scalar field is a slowly evolving component with negative pressure. This multifluid system can be described by the following action:

$$S = \int {\rm d}^4x\sqrt{-g}\,\left(-\frac{R}{2\kappa} + \mathcal{L}_{\rm m+r} + \frac{1}{2}\,g^{\mu\nu}\,\partial_\mu\varphi\,\partial_\nu\varphi - V(\varphi)\right), \quad (1)$$

where R is the Ricci scalar, $\mathcal{L}_{\rm m+r}$ is the Lagrangian density of matter and radiation, $\kappa = 8\pi\,G$, g is the determinant of a spatially flat Friedmann–Lemaître–Robertson–Walker (FLRW) metric tensor $g_{\mu\nu}$ and $V(\varphi)$ is the scalar field potential. We assume that any couplings to other fields are negligible so the scalar field interacts with other matter only through gravity. Minimizing the action with respect to the scalar field leads to its equation of motion

$$\ddot{\varphi} + 3H\dot{\varphi} + \frac{{\rm d}V(\varphi)}{{\rm d}\varphi} = 0, \quad (2)$$

where H is the Hubble parameter and we have assumed that the field is spatially homogeneous, $\varphi(\boldsymbol{x}, t) = \varphi(t)$. The impact of the background on the dynamics of φ is contained in the $3H\dot{\varphi}$ term. The Hubble parameter for dynamical dark energy in a flat universe is given by

$$\frac{H^2(z)}{H_0^2} = \left(\Omega_{\rm m}\,(1+z)^3 + (1-\Omega_{\rm m})e^{3\int_0^z {\rm d}\ln(1+z')\,[1+w(z')]}\right), \quad (3)$$

where H_0 and $\Omega_{\rm m} = \rho_{\rm m}/\rho_{\rm crit}$ are the values of the Hubble parameter and dimensionless matter density, respectively, at redshift

$z = 0$ and $\rho_{\rm crit} = 3H_0^2/(8\pi G)$ is the critical density. The dark energy equation of state is expressed as the ratio of the dark energy pressure to its energy density, denoted as $w = {\rm P}/\rho$. Once a standard kinetic term is assumed in the quintessence model, it is the choice of potential which determines w as

$$w = \frac{\dot{\varphi}^2/2 - V(\varphi)}{\dot{\varphi}^2/2 + V(\varphi)}\,. \tag{4}$$

In general, in these theories if the contribution from the kinetic ($\dot{\varphi} = 0$) and gradient energy ($\mathrm{d}\varphi/\mathrm{d}\boldsymbol{x} = 0$) is negligible, then the effect of the scalar field is equivalent to a cosmological constant which behaves as a perfect fluid, with $P = -\rho$ or $w = -1$.

2.1 Classes of quintessence models

Two broad classes of quintessence models can be used to solve both the fine-tuning and coincidence problems. The first is based on the idea of the so-called tracker fields (Steinhardt, Wang & Zlatev 1999). These fields adapt their behaviour to the evolution of the scalefactor and hence track the background density. The other class is referred to as 'scaling solutions' (Halliwell 1987; Wands, Copeland & Liddle 1993; Wetterich 1995). In these models, the ratio of energy densities, $\rho_\varphi/\rho_{\rm B}$, is constant.

In tracking models, the φ field rolls down its potential, $V(\varphi)$, to an attractor-like solution. The great advantage of these models is that this solution is insensitive to the initial conditions of the scalar field produced after inflation. A general feature of these tracking solutions is that as the scalar field is tracking behind the dominant matter component in the universe, its equation of state, w_φ, depends on the background component as

$$\frac{\rho_\varphi}{\rho_{\rm B}} = a^{3(w_{\rm B}-w_\varphi)}\,, \tag{5}$$

where $\rho_{\rm B}$ and $w_{\rm B}$ denote the background energy density and the equation of state, respectively, with $w_{\rm B} = 1/3$ (radiation era) and $w_{\rm B} = 0$ (matter era). As a result, the energy density of the scalar field remains subdominant during the radiation- and matter-dominated epochs, although it decreases at a slower rate than the background density. The quintessence field, ρ_φ, naturally emerges as the dominant component today and its equation of state is driven towards $w = -1$. An example of a tracking model is the inverse potential form proposed by Zlatev, Wang & Steinhardt (1999), $V(\varphi) \sim M^{4+\alpha}\varphi^{-\alpha}$, where M is a free parameter that is generally fixed by the requirement that the dark energy density today $\Omega_{\rm DE} \sim 0.7$ and so the quintessence potential must be $V \sim \rho_{\rm crit}$. This implies that φ is of the order of the Planck mass today, $\varphi \sim M_{\rm Pl}$. With $\alpha \leq 6$, the quintessence field equation of state is approximately $w_0 \leq -0.4$ today.

In scaling quintessence models, the ratio of energy densities, $\rho_\varphi/\rho_{\rm B}$, is kept constant, unlike tracking models, where ρ_φ changes more slowly than $\rho_{\rm B}$. During the evolution of the energy density in a 'scaling' model, if the dominant matter component advances as $\rho \propto a^{-n}$, then the scalar field will obey $\Omega_\varphi = n^2/\alpha^2$ after some initial transient behaviour. Scaling quintessence models can suffer from an inability to produce late-time acceleration, whilst at the same time adhering to observational constraints, such as the lower limit on Ω_φ during nucleosynthesis (Bean, Hansen & Melchiorri 2001). Albrecht & Skordis (2000) used a modified coefficient in their scaling potential, $V(\varphi) = V_{\rm p}{\rm e}^{-\lambda\varphi}$, where $V_{\rm p}(\varphi) = (\varphi - B)^\alpha + A$, resulting in a model which can produce late-time acceleration as well as satisfying cosmological bounds, for a variety of constants A and B. Barreiro, Copeland & Nunes (2000) considered a linear combination of exponential terms in the scalar field potential and found that this yielded a larger range of acceptable initial energy densities for φ compared with inverse models. Copeland, Nunes & Rosati (2000) also consider supergravity (SUGRA) corrections to quintessence models, where the resulting potential can exhibit either 'tracking' or 'scaling' behaviour depending on which path the scalar field takes down its potential towards the minimum where it would appear as a cosmological constant.

The physical origin of the quintessence field should be addressed by models motivated by high-energy particle physics. As the vacuum expectation value of the scalar field today is of the order of the Planck mass, any candidates for quintessence which arise in supersymmetric (SUSY) gauge theories may receive SUGRA corrections which will alter the field's potential. It is this fact that motivates many authors to argue that any quintessence model inspired by particle physics potentials must be based on SUGRA. Brax & Martin (1999) discuss such models and employ the potential $V(\varphi) = \Lambda^{4+\alpha}/\varphi^\alpha {\rm e}^{\kappa/2\varphi^2}$ with a value of $\alpha \geq 11$ in order to drive w_0 close to -1 today.

In summary, in this paper we will consider six quintessence models which cover the behaviours discussed above. In particular, INV1 and INV2, which are plotted in Fig. 1, have inverse power-law potentials and exhibit tracking solutions. The INV1 model is the 'INV' model considered by Corasaniti & Copeland (2003) and has a value of $w_0 = -0.4$ today. As current observational data favour a value of $w_0 < -0.8$ (Sanchez et al. 2009), the INV1 model will be used as an illustrative model. We shall consider a second inverse power-law model (INV2) which is in better agreement with the constraints on w. As noted by Corasaniti (2004), the scale Λ in the inverse power-law potential, $V(\varphi) = \Lambda^{\alpha+4}/\varphi^\alpha$, is fixed by the value of $\Omega_{\rm DE}$ today. Solving the coincidence problem requires this scale for Λ to be consistent with particle physics models. For values of $\alpha \geq 6$, it is possible to have energy scales of $\Lambda \sim 10^6$ GeV. Setting $\alpha = 6$ results in an equation of state with $w_0 = -0.4$ (INV1). It is possible

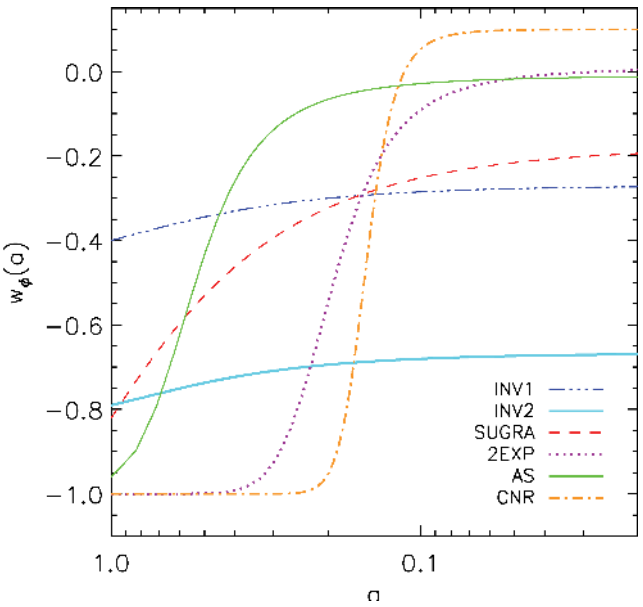

Figure 1. The dark energy equation of state as a function of the expansion factor, $w(a)$, for six quintessence models motivated by particle physics, which are either tracking or scaling solutions. The parametrization for $w(a)$ is given in equation (6) and the four parameter values which specify each model are given in Table 1. Note that the left-hand side of the x-axis is the present day.

to drive the equation of state closer to -1 today with lower values of α, although the value of Λ is then pushed to an undesirable energy range when compared with the typical scales of particle physics. The second model INV2, which has $w_0 = -0.79$ with $\alpha = 1$, has been added to illustrate a power-law potential with a dark energy equation of state which agrees with constraints found on w_0 using CMB, SN and large-scale structure data (Sanchez et al. 2009). We also use the SUGRA model of Brax & Martin (1999) which exhibits tracking field behaviour. The potential in this case also contains an exponential term which pushes the dark energy equation of state to $w_0 = -0.82$. The 2EXP model is an example of a scaling solution and features a double exponential term in the scalar field potential (Barreiro et al. 2000). The AS model suggested by Albrecht & Skordis (2000) belongs to the class of scaling quintessence fields. As mentioned previously, the parameters in this potential can be adjusted to have the fractional dark energy density, $\Omega_{\rm DE}$, below the nucleosynthesis bound in the early universe. The Copeland, Nunes & Rosati (CNR) model (Copeland et al. 2000) has a tracking potential where the scalar field rolls down to its minimum and will settle down to $w_0 = -1$ after a series of small oscillations.

Each of the quintessence models we consider is one of a family of such models with parameter values chosen in order to solve the issues of fine-tuning and coincidence, as well as to produce a value of $w_0 \sim -1$ today. These requirements limit the parameter space available to a particular quintessence potential. For example, this limits the range of the Brax & Martin (1999) SUGRA model. The SUGRA model we simulate has a fixed parameter value in the SUGRA potential but the dark energy equation of state for this model does not depend strongly on this parameter (see fig. 4 in Brax & Martin 1999).

2.2 Parametrization of w

Given the wide range of quintessence models in the literature it would be a great advantage, when testing these models, to obtain one model-independent equation describing the evolution of the dark energy equation of state without having to specify the potential $V(\varphi)$ directly. Throughout this paper we will employ the parametrization for w proposed by Corasaniti & Copeland (2003), which is a generalization of the method used by Bassett et al. (2002) for fitting dark energy models with rapid late-time transitions. Using a parametrization for the dark energy equation of state provides us with a model-independent probe of several dark energy properties. The dark energy equation of state, $w(a)$, is described by its value during radiation domination, $w_{\rm r}$, followed by a transition to a plateau in the matter-dominated era, $w_{\rm m}$, before making the transition to the present-day value w_0. Each of these transitions can be parametrized by the scalefactor $a_{\rm r,m}$ at which they occur and the width of the transition $\Delta_{\rm r,m}$.

In order to reduce this parameter space we use the shorter version of this parametrization for w, which is relevant as our simulations begin in the matter-dominated era. The equation for w valid after matter-radiation equality is

$$w_\varphi(a) = w_0 + (w_{\rm m} - w_0) \times \frac{1 + {\rm e}^{\frac{a_{\rm m}}{\Delta_{\rm m}}}}{1 + {\rm e}^{-\frac{a - a_{\rm m}}{\Delta_{\rm m}}}} \times \frac{1 - {\rm e}^{-\frac{a-1}{\Delta_{\rm m}}}}{1 - {\rm e}^{\frac{1}{\Delta_{\rm m}}}}. \qquad (6)$$

Corasaniti & Copeland (2003) showed that this four-parameter fit gives an excellent match to the exact equation of state. Table 1 gives the best-fitting values for the equation-of-state parameters for the different quintessence models taken from Corasaniti & Copeland (2003), with the addition of the INV2 model. The parametrization for the dark energy equation of state is plotted in Fig. 1 for the various quintessence models used in this paper.

Table 1. The equation of state of the dark energy models simulated, expressed in the parametrization of Corasaniti & Copeland (2003). The evolution of $w(a)$ is described by four parameters: the value of the equation of state today, w_0, and during matter-domination era, $w_{\rm m}$, the expansion factor, $a_{\rm m}$, when the field changes its value during matter domination and the width of the transition, $\Delta_{\rm m}$. We have added the INV2 model to this list as an example of an inverse power-law potential with a value of w_0 closer to -1 than in the INV1 model.

Model	w_0	$w_{\rm m}$	$a_{\rm m}$	$\Delta_{\rm m}$
INV1	-0.4	-0.27	0.18	0.5
INV2	-0.79	-0.67	0.29	0.4
SUGRA	-0.82	-0.18	0.1	0.7
2EXP	-1.0	0.01	0.19	0.043
AS	-0.96	-0.01	0.53	0.13
CNR	-1.0	0.1	0.15	0.016

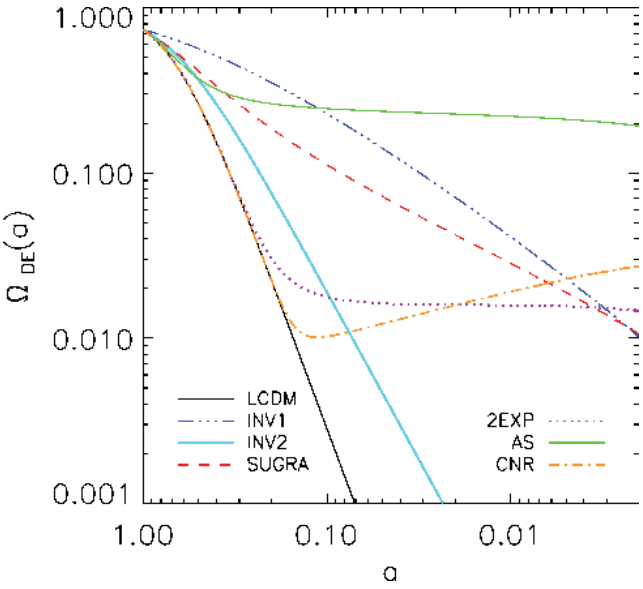

Figure 2. The dark energy density, $\Omega_{\rm DE}(a)$, as a function of the expansion factor. The INV1, SUGRA, CNR, 2EXP and AS models have significant levels of dark energy at early times. From $z \sim 9$ until today, the 2EXP and CNR models display the same energy density as ΛCDM. Note that the x-axis scale on this plot goes to $z > 300$ on the right-hand side.

Fig. 2 shows the evolution of the dark energy density with the expansion factor in each quintessence model. Some of these models display significant levels of dark energy at high redshifts in contrast to a ΛCDM cosmology. As the AS, CNR, 2EXP and SUGRA models have non-negligible dark energy at early times, all of these could be classed as 'early dark energy' models. As shown in Fig. 2, both the CNR and the 2EXP models have high levels of dark energy at high redshifts compared to ΛCDM; after an early rapid transition, the dark energy density evolves in the same way as in a ΛCDM cosmology. Other models, such as the AS, INV1 and SUGRA models, also have non-negligible amounts of dark energy at early times, and after a late-time transition, the dark energy density mimics a ΛCDM cosmology at very low redshifts. In Section 4 we will investigate if quintessence models which feature an early or late transition in their equation of state, and in their dark energy density, can be distinguished from ΛCDM by examining the growth of large-scale structure. The luminosity distance and Hubble

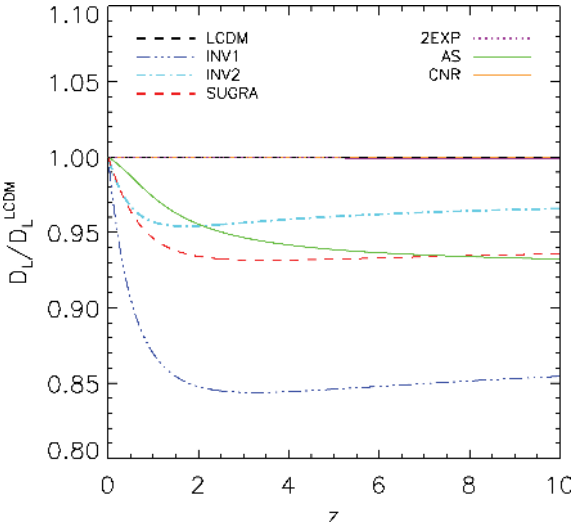

Figure 3. The luminosity distance in different quintessence models compared to that in a ΛCDM cosmology. In this case, we have assumed the same matter density of $\Omega_m = 0.26$ today in each of the models. The CNR and 2EXP models predict the same D_L as in ΛCDM and are overplotted.

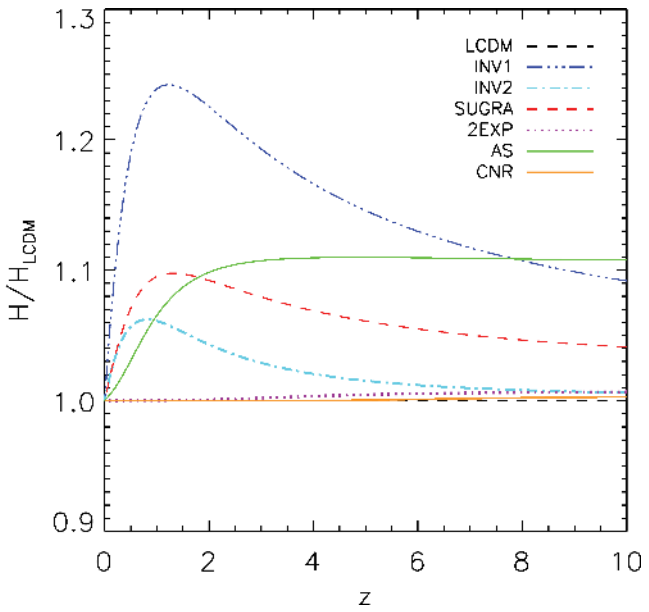

Figure 4. The ratio of the Hubble parameter for quintessence cosmologies to that in ΛCDM.

parameter in the quintessence models are compared to ΛCDM in Figs 3 and 4, respectively. In these plots, it is clear that the CNR and the 2EXP models differ from ΛCDM only at very high redshifts.

The adoption of a four-variable parametrization is essential to accurately model the expansion history over the full range of redshifts probed by the simulations. Using a one- or two-parameter equation of state whose application is limited to low-redshift measurements restricts the analysis of the properties of dark energy and cannot make use of high-redshift measurements such as the CMB. As an example, Corasaniti (2004) demonstrated that a two-parameter log expansion for $w(z)$, proposed by Gerke & Efstathiou (2002), can only take into account a quintessence model which varies slowly and cannot faithfully reproduce the original $w(z)$ at high redshifts. Bassett et al. (2004) analysed how accurately various parametrizations could reproduce the dynamics of quintessence models. They found that parametrizations based on an expansion to first order in z or $\log z$ showed errors of ∼10 per cent at $z = 1$. A general prescription for $w(z)$ containing more parameters than a simple one- or two-variable equation can accurately describe both slowly and rapidly varying equations of state (Bassett et al. 2004). For example, the parametrization provided by Corasaniti & Copeland (2003) can accurately mimic the exact time behaviour of $w(z)$ to <5 per cent for $z < 10^3$ using a four-parameter equation of state and to <9 per cent for $z < 10^5$ with a six-parameter equation. Finally, we note that the parametrization for w proposed by Corasaniti & Copeland (2003) is similar to the four-parameter equation of state in Linder & Huterer (2005) (Model 4.0) where the evolution of w is described in terms of the e-fold variable, $N = \ln a$, where a is the scalefactor.

2.3 The expected impact of dark energy on structure formation

The growth of structure is sensitive to the amount of dark energy, as this changes the rate of expansion of the Universe. As a result, a quintessence model with a varying equation of state could display different large-scale structures from a ΛCDM model. Varying the equation of state will result in different amounts of dark energy at different times. It has been shown that models with a larger density of dark energy at high redshift than ΛCDM have more developed large-scale structure at early times, when normalized to the same σ_8 today (Francis et al. 2008; Grossi & Springel 2009).

When the dark matter perturbations are small and the density contrast $\delta(\boldsymbol{x}, t) \ll 1$, the expression for the power spectrum as a function of time, $P(k, t)$, is separable as

$$P(k, t) = \frac{D(t)^2}{D(t_0)^2} P(k, t_0), \tag{7}$$

where $D(t_0)$ is the linear growth factor at the present epoch. The normalized growth factor $G = D/a$ obeys the following evolution equation (Linder & Jenkins 2003):

$$G'' + \left(\frac{7}{2} - \frac{3}{2}\frac{w(a)}{1 + X(a)}\right)\frac{G'}{a} + \frac{3}{2}\frac{1 - w(a)}{1 + X(a)}\frac{G}{a^2} = 0, \tag{8}$$

where

$$X(a) = \frac{\Omega_m}{1 - \Omega_m} e^{-3\int_a^1 \mathrm{d}\ln a' w(a')}, \tag{9}$$

and $w(a)$ is the dynamical dark energy equation of state. The linear growth factor for each quintessence model is plotted in Fig. 5. In Section 4.1, we present the simulation results for each quintessence model where the initial conditions were generated using a ΛCDM linear theory power spectrum and the background cosmological parameters are the best-fitting values assuming a ΛCDM cosmology (stage I). The difference between the simulations is the result of having a different linear growth rate for the dark matter perturbations.

The presence of small but appreciable amounts of dark energy at early times also modifies the growth rate of fluctuations from that expected in a matter-dominated universe and hence changes the shape of the linear theory $P(k)$ from the ΛCDM prediction. The quintessence scalar field can contribute at most a small fraction of the total energy density at early redshifts. Constraints on this amount come from big bang nucleosynthesis as well as from CMB measurements. Bean et al. (2001) found a limit of $\Omega_{DE} < 0.045$ at $a \sim 10^{-6}$ using the observed abundances of primordial nuclides and a constraint of $\Omega_{DE} < 0.39$ during the radiation-domination

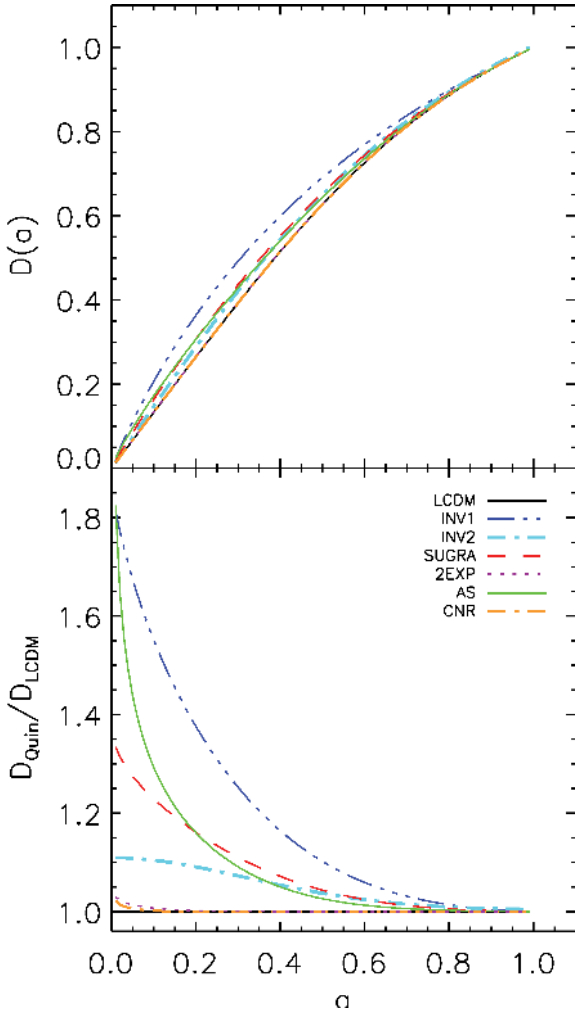

Figure 5. The growth factor as a function of the expansion factor. The upper panel shows the evolution of the linear growth factor in each quintessence model. In the lower panel, the ratio of the growth factor in the quintessence models compared to ΛCDM is plotted. The growth factor in each case has been normalized to unity today.

era, $a \sim 10^{-4}$, from CMB anisotropies. Caldwell et al. (2003) discuss the parameter degeneracies which allow for different amounts of dark energy at early times leaving the position of the CMB peaks unchanged (see Section 4.3). Using the *Wilkinson Microwave Anisotropy Probe* (*WMAP*) first-year data, Corasaniti et al. (2004) found a limit of $\Omega_{DE} < 0.2$ at $z \sim 10$. Some recent parametrization-dependent constraints on early dark energy models found the dark energy density parameter to be $\Omega_{DE} < 0.02$ at the last scattering surface (Xia & Viel 2009). Note that all of the models we consider are consistent with this constraint, except for the AS model (see Fig. 2).

If the dark energy is not a cosmological constant, then there will be dark energy perturbations present, δ_φ, whose evolution will affect the dark matter power spectrum and alter the evolution in equation (8) (Ferreira & Joyce 1998; Weller & Lewis 2003). As most of the quintessence models we will consider display a non-negligible contribution to the overall density from dark energy at early times, the matter power spectrum is affected in two ways (Ferreira & Joyce 1998; Caldwell et al. 2003; Doran, Robbers & Wetterich 2007). In the matter-dominated era, the growing mode solution for dark matter density perturbations is proportional to the expansion factor, $\delta_m \propto a$, in a universe without a scalar field component. In a dark energy model which has appreciable amounts of dark energy at early times, the dark matter growing mode solution on subhorizon scales is modified to become

$$\delta_m \propto a^{[\sqrt{25-24\Omega_{DE}}-1]/4}. \quad (10)$$

The growth of modes on scales $k > k_{eq}$, where k_{eq} is the wavenumber corresponding to the horizon scale at matter radiation equality, is therefore suppressed relative to the growth expected in a ΛCDM universe. For fluctuations with wavenumbers $k < k_{eq}$ during the matter-dominated epoch, the suppression takes place after the mode enters the horizon and the growing mode is reduced relative to a model with $\Omega_{DE} \simeq 0$. These two effects are illustrated for a scaling quintessence model in Ferreira & Joyce (1998), whose fig. 7 shows the evolution of δ_m for two wavenumbers: one that enters the horizon around $a_{eq}(k = 0.1\,\mathrm{Mpc}^{-1})$ and one that comes in during the radiation era ($k = 1\,\mathrm{Mpc}^{-1}$), in a universe with $\Omega_{DE} = 0.1$ during the matter-dominated era. There is a clear suppression of growth after horizon crossing compared to a universe with no scalar field. The overall result is a scale-independent suppression for subhorizon modes, a scale-dependent red tilt ($n_s < 1$) for superhorizon modes and an overall broadening of the turnover in the power spectrum. This change in the shape of the turnover in the matter power spectrum can be clearly seen in Fig. 6 for the AS model. This damping of the growth after horizon crossing will result in a smaller σ_8 value for the quintessence models compared to ΛCDM if normalized to CMB fluctuations (see also Kunz et al. 2004).

We have used the publicly available parametrized post-Friedmann (PPF) module for CAMB (Fang, Hu & Lewis 2008) to generate the linear theory power spectrum. This module supports a time-dependent dark energy equation of state by implementing a PPF prescription for the dark energy perturbations with a constant sound speed

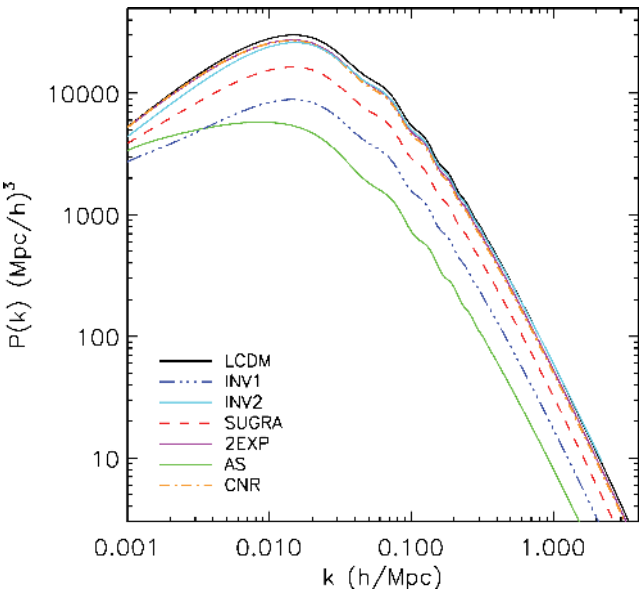

Figure 6. Linear theory power spectra at $z = 0$ for dynamical dark energy quintessence models and ΛCDM. In this plot, the spectra are normalized to CMB fluctuations (on smaller wavenumbers than are included in the plot). The presence of a non-negligible dark energy density fraction at early times causes a scale-independent suppression of growth for scales $k > k_{eq}$, where k_{eq} is the wavenumber corresponding to the horizon scale at matter radiation equality and a scale-dependent suppression at $k < k_{eq}$. Models with high Ω_{DE} at the last scattering surface have a lower σ_8 today compared to ΛCDM if normalized to CMB fluctuations.

$c_s^2 = 1$. Fig. 6 shows the dark matter power spectra at $z = 0$ generated by CAMB for each quintessence model and ΛCDM with the same cosmological parameters, an initial scalar amplitude of $A_s = 2.14 \times 10^{-9}$ and a spectral index $n_s = 0.96$ (Sanchez et al. 2009). As can be seen in this plot, models with higher fractional energy densities at early times have a lower σ_8 today and a broader turnover in $P(k)$. In Section 4.2, a consistent linear theory power spectrum was used for each quintessence model to generate the initial conditions for the simulations (stage II).

Finally, quintessence dark energy models will not necessarily agree with observational data when adopting the cosmological parameters derived assuming a ΛCDM cosmology. We consider how the different quintessence models affect various distance scales. We find the best-fitting cosmological parameters for each quintessence model using the observational constraints on distances such as the measurements of the angular diameter distance and sound horizon at the last scattering surface from the CMB. The method and data sets used are given in Appendix A and the corresponding simulation results which use a consistent linear theory power spectrum for each model together with the best-fitting cosmological parameters are presented in Section 4.3. (stage III).

3 SIMULATION DETAILS

We will determine the impact of quintessence dark energy on the growth of cosmological structures through a series of large N-body simulations. These simulations were carried out at the Institute of Computational Cosmology using a memory-efficient version of the TreePM code GADGET-2, called L-GADGET-2 (Springel 2005). As our starting point, we consider a ΛCDM model with the following cosmological parameters: $\Omega_m = 0.26$, $\Omega_{DE} = 0.74$, $\Omega_b = 0.044$, $h = 0.715$ and a spectral tilt of $n_s = 0.96$ (Sanchez et al. 2009). The linear theory rms fluctuation in spheres of a radius of $8\,h^{-1}$ Mpc is set to be $\sigma_8 = 0.8$. For each of the quintessence models, the parametrization for the dark energy equation of state given in equation (6) was used. In the first stage, we fix the cosmological parameters for all of the quintessence models to those of ΛCDM. As a result, some of the scalar field models do not match observational constraints on the sound horizon at the last scattering or the angular diameter distance. We shall discuss this further in Section 4.3 using the results given in Appendix A.

The simulations use $N = 646^3 \sim 269 \times 10^6$ particles to represent the dark matter in a computational box of a comoving length of $1500\,h^{-1}$ Mpc. We chose a comoving softening length of $\epsilon = 50\,h^{-1}$ kpc. The particle mass in the simulation is $9.02 \times 10^{11}\,h^{-1}\,M_\odot$ with a mean interparticle separation of $r \sim 2.3\,h^{-1}$ Mpc. The initial conditions of the particle load were set up with a glass configuration of particles. This arrangement is obtained by evolving a random distribution of particles with the sign of the gravitational force reversed (White 1994; Baugh, Gaztanaga & Efstathiou 1995). The particles are perturbed from the glass using the Zeldovich approximation which can induce small-scale transients in the measured power spectrum. These transients die away after $\simeq$10 expansion factors from the starting redshift (Smith et al. 2003). In order to limit the effects of the initial displacement scheme, we chose a starting redshift of $z = 200$.

The linear theory power spectrum used to generate the initial conditions was created using the CAMB package of Lewis & Bridle (2002). In the first stage of our calculations, presented in Section 4.1, the linear theory power spectrum used to set up the initial conditions in the quintessence models was the same as ΛCDM. For the purpose of computing the shape of $P(k)$ in stage I, we have assumed that the ratio of dark energy density to the critical density at the last scattering surface ($z_{lss} \sim 1000$) is negligible and have ignored any clustering of the scalar field dark energy. In Section 4.2, the linear theory $P(k)$ is generated for each quintessence model using a modified version of CAMB which incorporates the influence of dark energy on dark matter clustering at early times. In each model, the power spectra at redshift zero have been normalized to have $\sigma_8 = 0.8$. Using the linear growth factor for each dark energy model, the linear theory $P(k)$ was then evolved backwards to the starting redshift of $z = 200$ in order to generate the initial conditions for L-GADGET-2. Snapshot outputs of the dark matter distribution as well as the group catalogues were made at redshifts 5, 3, 2.5, 2, 1.5, 1, 0.75, 0.5, 0.25 and 0. The simulation code L-GADGET-2 has an inbuilt friends-of-friends (FOF) group finder which was applied to produce group catalogues of dark matter particles with 10 or more particles. A linking length of 0.2 times the mean interparticle separation was used in the group finder.

We investigate gravitational collapse in the six quintessence models listed in Table 1 by comparing the evolution of the power spectrum at various redshifts. The power spectrum was computed by assigning the particles to a mesh using the cloud in cell (CIC) assignment scheme (Hockney & Eastwood 1981) and then performing a fast Fourier transform on the density field. To restore the resolution of the true density field, this assignment scheme is corrected for by performing an approximate deconvolution (Baumgart & Fry 1991).

4 RESULTS

In the following sections, we present the power spectrum predictions from the three stages of simulations carried out as described in Section 2.3. The bottom line results are presented in Section 4.3, in which we compare power spectra in ΛCDM with a subset of dark energy models which also pass the currently available observational constraints. The reader pressed for time may wish to skip directly to this section. Sections 4.1 and 4.2 show intermediate steps away from ΛCDM towards the consistent dark energy models presented in Section 4.3, to allow us to understand the impact on $P(k)$. In Section 4.1, the Friedmann equation was modified with the quintessence model's equation of state as a function of redshift and a ΛCDM linear theory power spectrum was used to generate the initial conditions for all the simulations (stage I). In Section 4.2, we use a consistent linear theory power spectrum for each quintessence model (stage II). In Section 4.3 we constrain a set of cosmological parameters, using CMB, BAO and SN data, for each dark energy model. The final stage of simulations uses a consistent linear theory power spectrum for each model together with the best-fitting cosmological parameters (stage III).

4.1 Stage I: changing the expansion rate of the Universe

In this first stage of simulations, the same ΛCDM initial power spectrum and cosmological parameters were used for all models. In Fig. 7 we plot the power spectrum at redshifts $z = 0, 1, 5$ in ΛCDM (orange lines) and in the AS model (green lines), together with the linear theory power spectra for ΛCDM (black lines). The AS model has a linear growth rate that differs from ΛCDM by ∼20 per cent at $z = 5$. We also plot the Smith et al. (2003) 'Halofit' empirical fitting function for ΛCDM and the AS model. The Halofit function has been incorporated into the CAMB package, and this code was used to generate the output at various redshifts seen in Fig. 7. As this plot

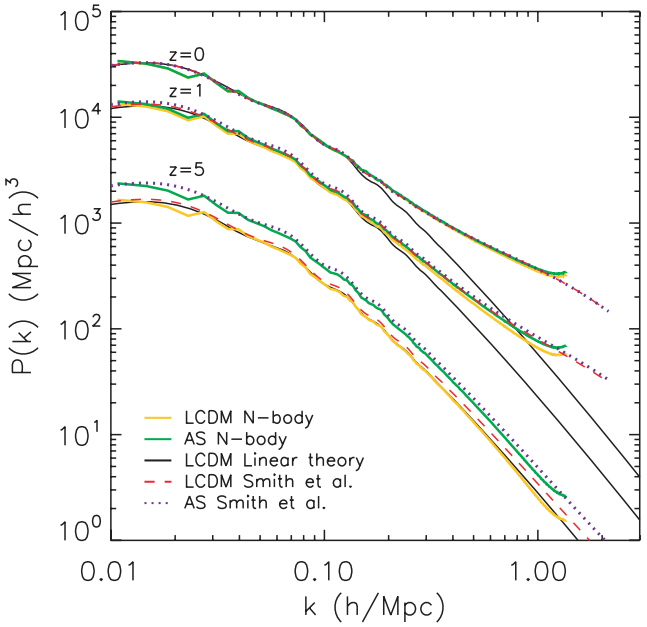

Figure 7. Power spectra in a ΛCDM cosmology (orange lines) and AS quintessence model (green lines) at redshift 0, 1 and 5. The red dashed lines corresponds to the Smith et al. (2003) analytical expression for the non-linear $P(k)$ in ΛCDM; the blue dotted lines show the equivalent for the AS model. The solid black line is the linear theory for ΛCDM at the corresponding redshift outputs. The Smith et al. (2003) expression for the AS model has been scaled with the appropriate growth factor for this model at each redshift.

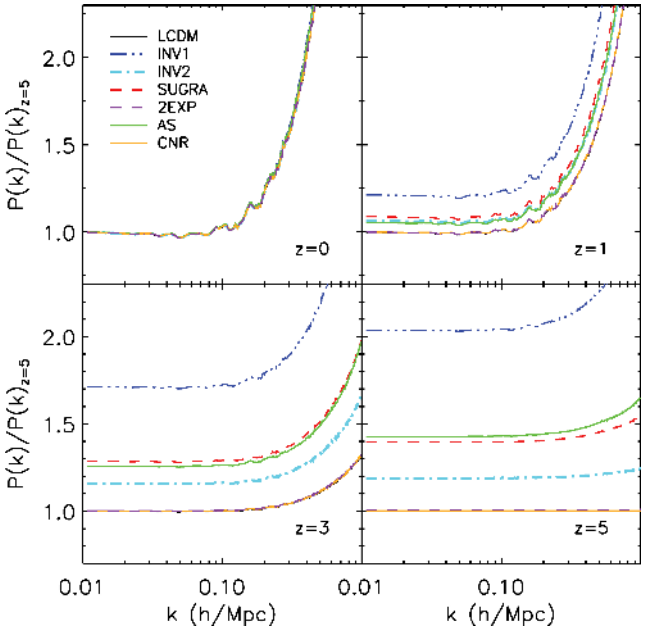

Figure 8. The non-linear growth of the power spectra in the various quintessence models as indicated by the key in the top left-hand panel. Each panel shows a different redshift. The power spectra in each case have been divided by the ΛCDM power spectrum at redshift 5 scaled to take out the difference between the ΛCDM growth factor at $z = 5$ and the redshift plotted in the panel. This removes the sampling variance due to the finite box size and highlights the enhanced non-linear growth found in quintessence cosmologies compared to ΛCDM. A deviation of the power ratio from unity therefore indicates a difference in $P(k)$ from the linear perturbation theory of ΛCDM.

shows, the Smith et al. (2003) expression accurately describes the evolution of the power spectrum at redshift 0 in both models and at earlier times. As the normalization and linear spectral shape is the same in these two models, Halofit accurately reproduces the non-linear power in each model at various redshifts once the appropriate linear growth factor for the dark energy model at that redshift is used. The Smith et al. expression agrees with the simulation output at $z = 0$ to within 4 per cent for $k < 1\,h\,\mathrm{Mpc}^{-1}$ for both the quintessence model and ΛCDM. At higher redshifts, the difference between the simulation output and the Halofit prediction for all the models is just under 10 per cent on scales $k < 0.3\,h\,\mathrm{Mpc}^{-1}$ at $z = 5$.

To highlight the differences in the power between the different models, we plot in Fig. 8 the measured power divided by the power at $z = 5$, after scaling to take into account the difference in the linear theory growth factors for the output redshift and $z = 5$, for ΛCDM. This removes the sampling variance from the plotted ratio (Baugh & Efstathiou 1994). A ratio of unity in Fig. 8 would indicate linear growth at the same rate as expected in ΛCDM.

Fig. 8 shows four epochs in the evolution of the power spectrum for all of the quintessence models and ΛCDM. The black line in the plot shows the $P(k)$ ratio for ΛCDM (note that the yellow curve for the CNR model is overplotted). Non-linear growth can be seen as an increase in the power ratio on small scales, $k > 0.3\,h\,\mathrm{Mpc}^{-1}$ at $z = 3$ and $k > 0.1\,h\,\mathrm{Mpc}^{-1}$ at $z = 0$. Four of the quintessence models (INV1, INV2, SUGRA and AS) differ significantly from ΛCDM for $z > 0$. These models show advanced structure formation, i.e. more power than ΛCDM, and a large increase in the amount of non-linear growth. All models are normalized to have $\sigma_8 = 0.8$ today and as a result all the power spectra are very similar at redshift zero in Fig. 8. There are actually small differences between the quintessence models at $z = 0$ as seen on the expanded scale in Fig. 9. This increase in non-linear power at small scales in the quintessence models is due to the different growth histories.

The power spectra predicted in the 2EXP and CNR models show minor departures from that in the ΛCDM cosmology. This is expected as Figs 1 and 2 show that the equations of state and the dark energy densities in these two models are the same as ΛCDM at low redshifts and all three simulations begin from identical initial conditions. It could be possible to distinguish these two models from the concordance cosmology at higher redshifts if we do not ignore the dark energy perturbations or changes in the growth factor which alter the form of the linear theory power spectrum. We shall discuss this more in the next stage of our simulations in Section 4.2.

Finally, we investigate if the enhanced growth in the power spectrum seen in Fig. 8 in the quintessence models is due solely to the different linear growth rates at a given redshift in the models. In order to test this idea, the power spectrum in a quintessence model and ΛCDM are compared not at the same redshift but at the same linear growth factor.[1] As the growth rates in some of the quintessence models are very different from that in the standard ΛCDM cosmology, the power spectra required from the simulation will be at different output redshifts in this comparison. For example, the normalized linear growth factor is $D = 0.5$ at a redshift of $z = 1.58$ in a ΛCDM model and has the same value at $z = 1.82$ in the SUGRA model, at $z = 1.75$ in the AS model and at $z = 2.25$ in the INV1 quintessence model. In Fig. 10 we show the power spectrum of simulation outputs from the INV1, AS, SUGRA and CNR models divided by the power spectrum output in ΛCDM at the same linear

[1] We thank S. D. M. White for this suggestion.

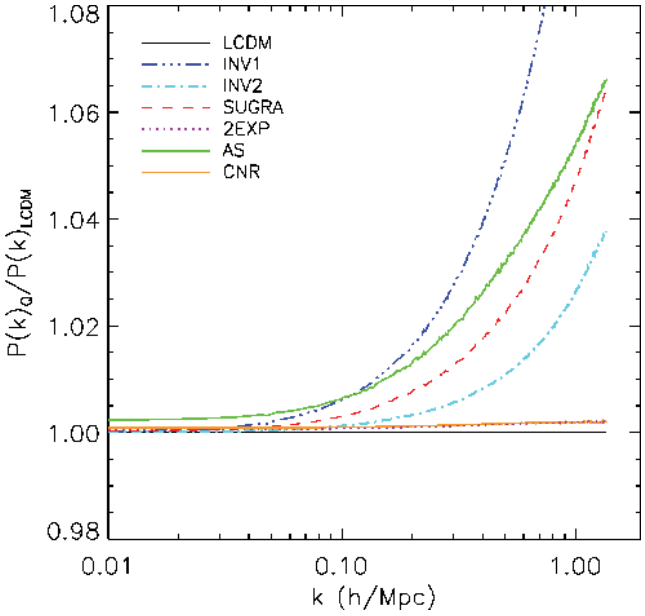

Figure 9. Ratio of power spectra output from the simulations in the six quintessence models compared to the non-linear ΛCDM $P(k)$ at redshift 0. Note the expanded scale on the y-axis. As expected, the 2EXP and CNR models show no difference from ΛCDM while the difference in the INV1, INV2, SUGRA and AS models is under 10 per cent for wavenumbers $k < 1\,h\,\mathrm{Mpc}^{-1}$.

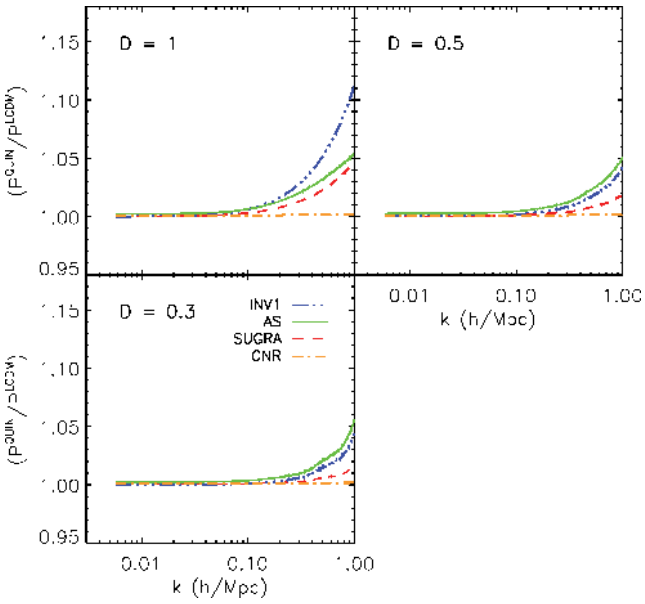

Figure 10. The ratio of the quintessence model power spectra to the ΛCDM power spectrum output from the simulations at three values of the linear growth factor $D = 1$, $D = 0.5$ and $D = 0.3$. Each panel shows the results of this exercise for the AS, CNR, 2EXP and SUGRA quintessence models. The growth factors correspond to $z = 3.4$ ($D = 0.3$), $z = 1.6$ ($D = 0.5$) and $z = 0$ ($D = 1$) for ΛCDM. For each model, the choice of growth factor corresponds to slightly different redshifts, with the biggest difference being for the INV1 model. A ratio of unity would indicate that the growth factor is the only ingredient needed to predict the power spectrum in the different quintessence models. Note the expanded scale on the y-axis.

growth rate. We ran the simulations taking three additional redshift outputs where the linear growth rate had values of $D = 1$, $D = 0.5$ and $D = 0.3$. It is clear from Fig. 10 that scaling the power spectrum in this way can explain the enhanced linear and most of the excess non-linear growth seen in Fig. 8 for scales $k < 0.1\,h\,\mathrm{Mpc}^{-1}$. For example, in the INV1 model the enhanced non-linear growth, on scales $k \sim 0.3\,h\,\mathrm{Mpc}^{-1}$ at fixed $D = 0.3$, differs from ΛCDM by at most 5 per cent in Fig. 10 as opposed to at most 30 per cent at $z = 5$ in Fig. 8. At earlier redshifts when the linear growth rate is $D = 0.3$, the non-linear growth in the quintessence models agrees with ΛCDM on smaller wavenumbers $k < 0.3\,h\,\mathrm{Mpc}^{-1}$. As in Fig. 8, the CNR model shows no difference from ΛCDM when plotted in this way.

Note in Fig. 10 that the INV1 model has less non-linear growth at $D = 0.3$ and $D = 0.5$ compared to the AS model. The AS and SUGRA models have a growth rate of $D = 0.5$ at lower redshifts compared to the INV1 model and so are at a later stage in their growth history. The INV1 model has a growth rate of $D = 0.5$ at $z = 2.25$ whereas for the AS model this occurs at $z = 1.75$ and at 1.82 for the SUGRA model. The reason for the success of this simple model – matching the growth factor to predict the clustering – can be traced to the universality of the mass function, which we discuss in Section 4.4. In this stage I calculation, the models have the same mass function when plotted at the epoch corresponding to a common growth factor. This means that the two-halo contribution to the clustering is therefore the same. Can this simple halo picture of the clustering also explain the clustering on small scales (high k)? Although the abundance of haloes in the models is the same at the epochs corresponding to a given value of the growth factor, the concentrations of the haloes will not be the same. In cosmologies where the haloes formed at a higher redshift (i.e. roughly the redshift corresponding to a particular value of D), one would expect these haloes to have higher concentrations than their counterparts in the other models (Eke, Navarro & Steinmetz 2001). A higher concentration would be expected to yield stronger non-linear clustering and hence more power at high k in Fig. 10. Unfortunately, our simulations do not have the resolution to probe the required range of wavenumbers to uncover this behaviour. The ratios plotted in Fig. 10 stop at wavenumbers approximately equivalent to the collapsed radius of a massive halo.

Hence, it seems that scaling the power spectrum using the linear growth rate can be used to predict the linear growth in the quintessence dark energy simulations and can reproduce some of the non-linear growth at early redshifts. In Fig. 10, there are still some differences in the small-scale growth in quintessence models compared to ΛCDM which cannot be explained by the different linear growth rates. We find that non-linear evolution is not just a function of the current value of the linear growth rate but also depends on its history through the evolution of the coupling between long- and short-wavelength modes.

4.2 Stage II: use of a self-consistent linear theory $P(k)$

We have again run the simulations presented in the previous section but this time using the appropriate linear theory $P(k)$ for each model (shown in Fig. 6) normalized to $\sigma_8 = 0.8$ today (stage II). After normalizing the power spectra in this way, the difference between the quintessence models $P(k)$ and ΛCDM can be seen in Fig. 11. The INV2 model was not included in this set of simulations as there is a negligible difference in the linear theory power spectrum from ΛCDM. Note that Francis et al. (2008) also generate the linear theory power spectrum for 'early dark energy' models and

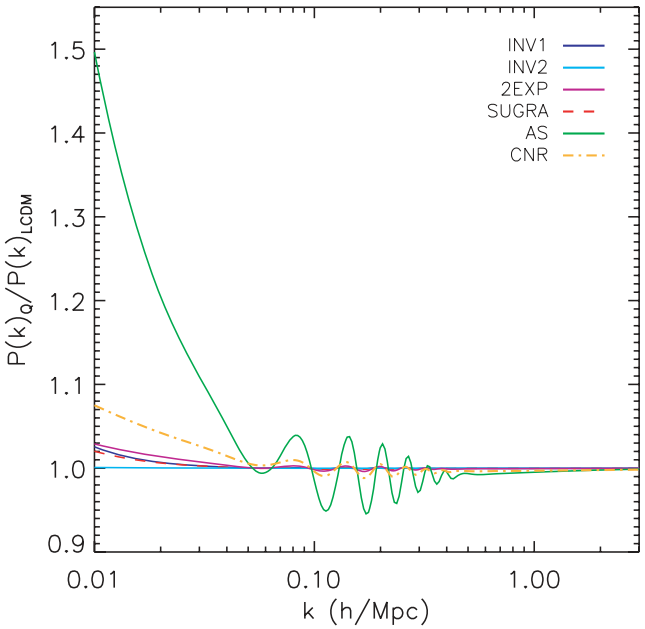

Figure 11. Ratio of linear theory power spectra for quintessence models shown in Fig. 6 to that in ΛCDM. In this plot, each $P(k)$ has been normalized so that $\sigma_8 = 0.8$ today; this is the normalization used in our simulations.

normalize all $P(k)$ to have the same σ_8 today. Francis et al. (2008) make a equivalent plot to Fig. 11 but find a decrease in this ratio with decreasing scale ($k > 0.2\,h\,\mathrm{Mpc}^{-1}$), using the parametrization for early dark energy proposed by Doran & Robbers (2006), in contrast to the ratio of unity we find on small scales in Fig. 11. This difference is due to the different parametrizations used for the dark energy equation of state, as a ratio of unity is obtained on small scales for the same 'early dark energy' model using the parametrization suggested by Wetterich (2004) (Francis, private communication).

In the first row of Fig. 12 we plot the power spectrum for the stage II SUGRA model at $z = 0$, 1 and 3 divided by the simulation output in ΛCDM at $z = 5$ as in Fig. 8 (red dashed lines). The result from Fig. 8, stage I SUGRA, is also plotted here to highlight how changing the spectral shape affects the non-linear growth in the simulations. On large scales, the growth is not modified by the altered spectral shape. The growth of perturbations on small scales in the simulation is affected by the modified linear theory used in the initial conditions. Normalizing the power spectra to $\sigma_8 = 0.8$ results in more power on large scales in the quintessence models compared to ΛCDM, as can be seen in Fig. 11. This enhanced large-scale power couples to the power on smaller scales and results in a small increase in the non-linear power spectrum for $k > 0.1\,h\,\mathrm{Mpc}^{-1}$ in the stage II SUGRA simulation compared to the one using ΛCDM linear theory $P(k)$ in stage I.

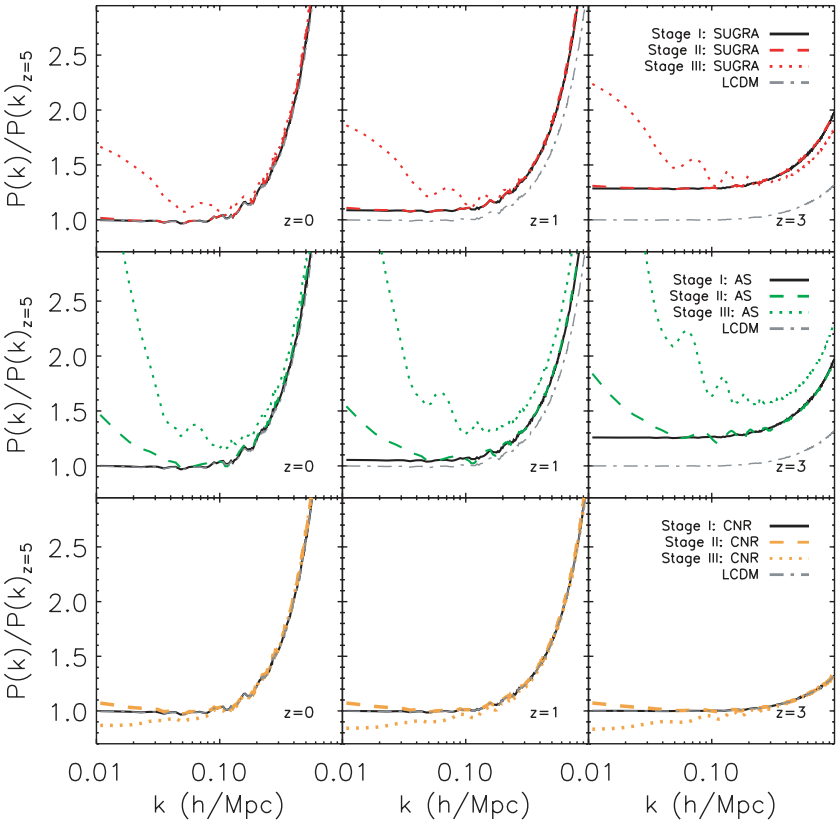

Figure 12. Ratios of power spectra for the SUGRA (first row), AS (second row) and CNR (third row) quintessence models compared to ΛCDM from the three stages of simulations in this paper. The plot shows the growth in the quintessence models using ΛCDM linear theory $P(k)$ in the initial conditions in black (stage I) and using a self-consistent linear theory $P(k)$ for each quintessence model (dashed coloured line) (stage II). The dotted lines shows the $P(k)$ ratio from the simulation for the quintessence models using the best-fitting parameters in Table A3 (stage III). The power spectra in each case have been divided by the ΛCDM power spectrum at redshift 5 with appropriate scaling of ΛCDM growth factors. The linear theory power spectra in each case have been normalized to $\sigma_8 = 0.8$.

In the second row of Fig. 12, we plot the power spectrum for the stage II AS model as green dashed lines at $z = 0$, 1 and 3 divided by the simulation output in ΛCDM at $z = 5$ as in Fig. 8. The growth of dark matter perturbations is greatly suppressed in the AS model due to the large fractional dark energy density at high redshifts. After fixing $\sigma_8 = 0.8$, there is more power on large scales in the AS model compared to ΛCDM. As in the first row of Fig. 12, there is a small increase in non-linear power for the AS model in stage II. Although the excess large-scale power is significantly larger than in the SUGRA model case, it does not result in more non-linear power on small scales through mode coupling, as can be seen in the panels in the second row in Fig. 12. The linear theory power spectrum for these quintessence models has a scale-dependent red tilt on large scales which shifts the position of the BAO peaks which is the origin of the oscillation apparent in the second row of Fig. 12 at $z = 3$. The difference in BAO peak positions is very prominent when we plot the ratio of the power spectrum in the AS model to the ΛCDM power spectrum and can be clearly seen in Fig. 12.

4.3 Stage III: consistency with observational data

In this section we present the power spectra results in ΛCDM and a subset of the dark energy models, measured from simulations which use a consistent linear theory power spectrum for each model together with the best-fitting cosmological parameters. We have simulated the SUGRA, AS and CNR models using the best-fitting cosmological parameters from Table A3 and the linear theory power spectrum specific to each model as discussed in Section 2.3. We chose to simulate these three models following the analysis and results of Sections 4.1, 4.2 and Appendix A. Any of the dark energy models listed in Section 2.2 which showed similar results in Section 4.2 to ΛCDM and similar cosmological parameters in Appendix A have not been simulated again.

Table A3 shows the best-fitting values for $\Omega_{\rm m}h^2$, $\Omega_{\rm b}h^2$ and H_0 for each quintessence model, found by minimizing $\chi^2_{\rm total} = \chi^2_{WMAP+{\rm SN}+{\rm BAO}}$. The SUGRA, AS and CNR models had the biggest improvement in the agreement with observational constraints, on allowing $\Omega_{\rm m}h^2$, $\Omega_{\rm b}h^2$ and H_0 to vary. The results for the SUGRA, AS and the CNR model are shown as dotted coloured lines in Fig. 12 and are referred to as stage III in the legend to distinguish them from the results of Sections 4.1 and 4.2 which are also plotted. In each row, we show the simulation outputs at $z = 0$, 1 and 3. The simulation results for each quintessence model use the models' linear theory and the best-fitting parameters from Table A3. Using the best-fitting parameters for each model together with the correct linear theory changes the growth of structure in the simulation.

In Fig. 12, the measured power spectrum for each model is divided by the power for ΛCDM at $z = 5$ which has been scaled using the difference in the linear growth factor between $z = 5$ and the redshift shown. Plotting the ratio in this way highlights the differences in growth between the quintessence models and ΛCDM as well as removing sampling variance.

The measured power for the SUGRA model is plotted in the first row in Fig. 12. The power spectra have all been normalized to $\sigma_8 = 0.8$ resulting in a large increase in the large-scale power ($k < 0.1\,h\,{\rm Mpc}^{-1}$) seen in Fig. 12 compared to ΛCDM. There is a large increase in the linear and non-linear growth in this model at $z > 0$ (dotted red line) compared to ΛCDM (dot–dashed grey line). The second row in Fig 12 shows that there is a significant enhancement in the growth in the AS power spectrum measured compared to ΛCDM for $z < 3$. The power measured from the simulations of the CNR model are plotted in the third row of Fig. 12. We find that there is a small reduction in the amount of linear and non-linear growth in this model compared to ΛCDM.

In Fig. 12, we also plot the simulation results for these three models from Section 4.1 (stage I), where ΛCDM linear theory was used in the initial conditions (black lines). The dashed coloured lines show the simulation results from Section 4.2 (stage II), where the quintessence model linear theory was used. The SUGRA power spectrum measured in stage III has less non-linear growth at high redshifts compared to the SUGRA $P(k)$ from stage I or II due to changes in the spectral shape. The measured power for the AS model using the best-fitting parameters (stage III) shows enhanced growth on all scales compared to the power for the AS model in stage I [using ΛCDM parameters and linear theory $P(k)$] or stage II (using ΛCDM parameters).

These results show the importance of each of the three stages in building up a complete picture of a quintessence dark energy model. Models whose equation of state is very different from ΛCDM at low redshifts, for example the SUGRA and the AS model, show enhanced non-linear growth today compared to ΛCDM. Models whose equation of state is very different to ΛCDM only at early times, for example the CNR model, will show no difference in the non-linear growth of structure if we use the ΛCDM spectral shape (stage I). In stages II and III, the shape of the power spectrum in the CNR model has changed and is very different to ΛCDM on large scales as can be seen in Fig. 12. Using the best-fitting cosmological parameters for this model, we find a very small reduction (<2 per cent) in the non-linear growth at $z = 0$ compared to ΛCDM.

4.4 Mass function of dark matter haloes

In this section, we present the mass function of dark matter haloes in the quintessence models using the three stages of simulations discussed in Sections 4.1–4.3, respectively.

Press & Schechter (1974, hereafter P-S) proposed an analytical expression for the abundance of collapsed objects with mass M in the range M to $M + {\rm d}M$ at redshift z, based on the spherical collapse model in which a perturbation can be associated with a virialized object at $z = z'$, if its density contrast, extrapolated to $z = z'$ using linear theory, exceeds some threshold value, $\delta_{\rm c}$, the critical linear density contrast. It has been shown that the P-S approach fails to reproduce the abundance of haloes found in simulations, overpredicting the number of haloes below the characteristic mass M_* and underpredicting the abundance in the high-mass tail (Efstathiou & Rees 1988; White, Efstathiou & Frenk 1993; Lacey & Cole 1994; Eke, Cole & Frenk 1996; Governato et al. 1999).

It is thought that the main cause of this discrepancy is the spherical collapse approximation, as the perturbations in the density field are inherently triaxial. After turnaround, each axis may evolve separately until the final axis collapses and the object virializes. Sheth, Mo & Tormen (2001) and Sheth & Tormen (2002, hereafter S-T) modified the P-S formalism, replacing the spherical collapse model with ellipsoidal collapse, in which the surrounding shear field as well as the initial overdensity determines the collapse time of an object. Sheth et al. (2001) found a universal mass function for any CDM model. Jenkins et al. (2001) found a universal empirical fit to the form of the mass function measured from a suite of cosmological simulations. The Jenkins et al. mass function can accurately predict halo abundances over a range of cosmologies and redshifts (see also Warren et al. 2006; Reed et al. 2007; Crocce et al. 2009).

We use a FOF halo finder, with a constant linking length of $b = 0.2$, to identify haloes in all cosmologies. In Fig. 13, we plot groups containing 20 particles or more to ensure that the

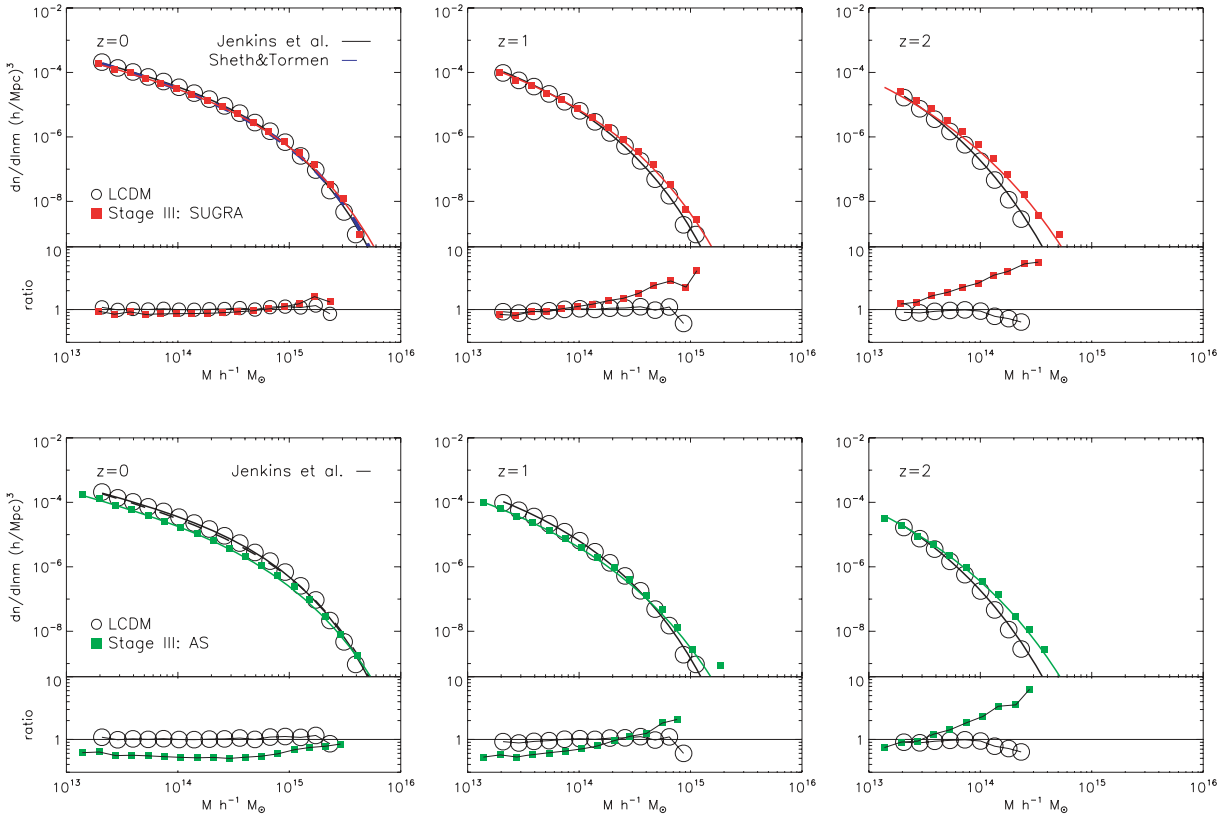

Figure 13. Dark matter halo mass functions for the SUGRA (first row) and AS (second row) quintessence models compared with that in ΛCDM from the stage III simulations at $z = 0$, 1 and 2. The mass function in ΛCDM is shown as open black circles throughout this plot. In the first row, the red filled squares show the mass function from the simulation for the SUGRA model using the best-fitting parameters in Table A3 (stage III). Underneath each panel in the first row, we plot the log of the ratio of the measured mass function for ΛCDM (open black circles) and stage III SUGRA (red squares) to the Jenkins mass function for ΛCDM. In the second row, the green filled squares show the mass function from the simulation for the AS model using the best-fitting parameters in Table A3 (stage III). For the AS stage III simulation, $\Omega_{\rm m}h^2 = 0.086$, giving rise to a change in the spectral shape of the linear theory power spectrum. As a result, there are fewer low-mass haloes and a similar number of high-mass haloes at $z = 0$ compared to ΛCDM ($\Omega_{\rm m}h^2 = 0.1334$). The difference between the Jenkins et al. mass function for ΛCDM and the measured mass function for ΛCDM (open black circles) and stage III AS (green squares) is plotted underneath each panel in the second row. The black horizontal line indicates a ratio of unity in the ratio plots. In the first and second rows, the solid black (red/green) lines are the predicted abundances in the ΛCDM (SUGRA/AS) model using the Jenkins et al. fitting function at various redshifts. In the top left-hand panel, for reference, we have also plotted the Sheth & Tormen mass function (blue dashed line) for ΛCDM.

systematic uncertainties in the mass function are at or below the 10 per cent level; tests show that 90 per cent or more of such haloes are gravitationally bound (Springel et al. 2005). The first row in Fig. 13 shows the mass function for SUGRA and ΛCDM at $z =$ 0, 1 and 2. The filled red squares represent the mass function from stage III of the simulations where a consistent linear theory and cosmological parameters were used for the SUGRA model. The mass function for ΛCDM (open black circles) and the SUGRA model are plotted together with the Jenkins et al. mass function shown in black (red) for ΛCDM (SUGRA). The S-T mass function is shown in the top left-hand panel in the first row of this figure (blue dashed line) for comparison. The abundances in both ΛCDM and SUGRA agree with each other at redshift 0 and with the Jenkins et al. and S-T models, although the fitting formulae seem to slightly underpredict the number of haloes at the high-mass end ($M > 10^{15}\,h^{-1}\,{\rm M}_{\odot}$). In the first row of Fig. 13, the number of haloes in the two models start to differ at $z = 1$, and at $z = 2$ there is a large difference in the mass functions. The linear growth factor for the SUGRA model together with the best-fitting cosmological parameters from Table A3 have been used to obtain the Jenkins et al. fit at the earlier redshifts. The Jenkins et al. fit describes the data slightly better at the high-mass end at higher redshifts than the S-T prescription. This is as expected as the Jenkins et al. fit was explicitly tested at the high-mass end of the mass function. Each model shows only small (<20 per cent) differences between the measured value and the Jenkins et al. fitting formula for $M < 10^{15}\,h^{-1}\,{\rm M}_{\odot}$ at $z = 0$. Underneath each panel in the first row in Fig. 13, we plot the ratio between the measured mass function for ΛCDM and the SUGRA model in stage III, and the Jenkins at al. mass function for ΛCDM.

The second row of Fig. 13 repeats this comparison for the AS model. In this row the mass function for ΛCDM (open black circles) and the AS model from stage III (green squares) of the simulations at $z = 0$, 1 and 2 are plotted. The Jenkins et al. mass function for ΛCDM (black line) and the AS model for stage III (green line) are also plotted. The AS model has a greater abundance of haloes than ΛCDM at $z = 2$. For the stage III simulation, the AS model has $\Omega_{\rm m}h^2 = 0.086$ giving rise to a change in the spectral shape of the linear theory power spectrum from ΛCDM linear theory ($\Omega_{\rm m}h^2 = 0.133$). As a result there are fewer low-mass haloes and a similar number of high-mass haloes at $z = 0$ compared to ΛCDM. This change accounts for the decrease in the mass function for $M < 10^{15}\,h^{-1}\,{\rm M}_{\odot}$ seen at $z = 0$ in the AS model (green squares). At $z = 0$, there are only small (<20 per cent) differences between the measured value and the Jenkins et al. fitting formula for $M < 10^{15}\,h^{-1}\,{\rm M}_{\odot}$ for

ΛCDM and the AS model from stage III. The ratio of the Jenkins et al. mass function for ΛCDM to the measured mass function for ΛCDM and the AS model from stage III is plotted underneath each panel in the second row in Fig. 13.

Only the SUGRA and AS models are plotted in Fig. 13 but similar differences in halo abundances are seen in the INV models compared to ΛCDM, whilst only negligible differences with ΛCDM were found in the mass functions of 2EXP and CNR. Grossi & Springel (2009) found similar results for the mass function over the range 10^{11}–$10^{14}\,h^{-1}\,\mathrm{M}_{\odot}$ in an 'early dark energy' model, using much smaller volume simulations than ours. They found a higher number density of haloes corresponding to groups and clusters in non-standard dark energy models at high redshifts compared to ΛCDM, while at $z = 0$ all the models agreed with one another. We find similar results although using the cosmological parameters from Table A3 for each quintessence model can give different abundances at $z = 0$ in those models compared to ΛCDM because although σ_8 is the same the shape of the linear theory can be different. Also, we have been able to probe a higher mass range for the dark matter haloes. The high-mass end of the mass function is very sensitive to changes in the current value of the linear growth factor in the different cosmologies.

In Fig. 14, we plot the fraction of the total mass in haloes of mass M rather than simply the abundance as shown in Fig. 13. We compare the Jenkins et al. analytic fit to our simulated halo mass functions in the SUGRA and AS models and in ΛCDM at $z = 0$ and 1 in Fig. 14. In this plot the quantity $\ln \sigma^{-1}(M, z)$ is used as the mass variable instead of M, where $\sigma^2(M, z)$ is the variance of the linear density field at $z = 0$. This variance can be expressed as

$$\sigma^2(M, z) = \frac{D^2(z)}{2\pi^2} \int_0^\infty k^2 P(k) W^2(k; M) \mathrm{d}k \,, \qquad (11)$$

where $W(k; M)$ is a top hat window function enclosing a mass M, $D(z)$ is the linear growth factor of perturbations at redshift z and $P(k)$ is the power spectrum of the linear density field. Plotting different masses at different redshifts in this way takes out the redshift dependence in the power spectrum. Note that a large value of $\ln \sigma^{-1}(M, z)$ corresponds to a rare halo. Using this variable, Jenkins et al. found that the mass function at different epochs has a universal form, for a fixed power spectrum shape. Note that in our case, the stage III simulations have somewhat different power spectra, which account for the bulk of the dispersion between the simulation results at the rare object end of Fig. 14; in stage I, the simulation results agree with the Jenkins et al. universal form to within 25 per cent at $\ln \sigma^{-1} = 1.0$. As shown in Fig. 14, we find that the Jenkins et al. fitting formula is accurate to ∼20 per cent at $z = 0$ for all the models in the range $M < 10^{15}\,h^{-1}\,\mathrm{M}_{\odot}$. At higher redshifts, the measured mass function for the SUGRA model and ΛCDM differs from the Jenkins et al. mass function by ∼30 per cent over the same mass range while for the AS model the difference is ∼50 per cent at $z = 1$. In previous work, Linder & Jenkins (2003) also found that the predicted mass function for a SUGRA–QCDM simulation, which would be the equivalent of our stage I simulations, was well fitted (within 20 per cent) by the Jenkins et al. formula.

4.5 The appearance of baryonic acoustic oscillations in quintessence models

In this section, we examine the BAO signal in the matter power spectrum for the AS, SUGRA and CNR models. Angulo et al. (2008) presented a detailed set of predictions for the appearance of the BAO signal in the ΛCDM model, covering the impact of non-linear growth, peculiar velocities and scale-dependent redshift-space distortions and galaxy bias. Here we focus on the first of these effects and show power spectra in real space for the dark matter. We do not consider the INV1 model as it is not consistent with observational constraints (Appendix A), or the INV2 or 2EXP models as they are indistinguishable from ΛCDM, and hence were not simulated again in stage III (Section 4.3).

In stage I of our simulations (Section 4.1), we would expect the linear theory comoving BAO for the quintessence models to be identical to ΛCDM as the same linear theory power was used for all models. In stage II (Section 4.2), some of the quintessence models have large amounts of dark energy at early times which will alter the sound horizon in these models compared to ΛCDM (see Table A3), and as a result we would expect to see a corresponding shift in the BAO peak positions. The best-fitting cosmological parameters found in stage III were derived using CMB, BAO and SN distance measurements (see Appendix A). Stage III of our simulations (Section 4.3) uses these parameters and we would expect models with the same BAO distance measures to have the same peak pattern in the matter power spectrum as ΛCDM.

The BAO are approximately a standard ruler and depend on the sound horizon, r_s, given in equation (A3) (Sanchez, Baugh & Angulo 2008). The apparent size of the BAO scale depends on the distance to the redshift of observation and on the ratio r_s/D_v, where D_v is an effective distance measure which is a combination

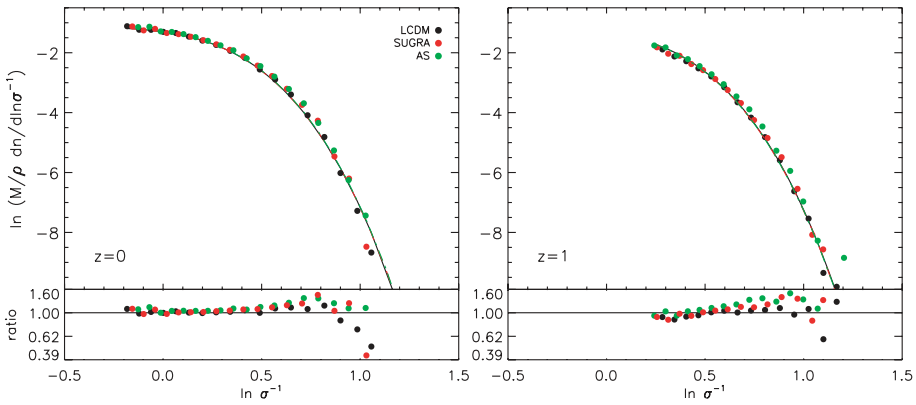

Figure 14. The halo mass function for the SUGRA and AS model and ΛCDM at $z = 0$ and 1 compared to the Jenkins et al. (2001) analytic fit. The Jenkins et al. mass function is plotted as solid black (red/green) lines for ΛCDM (SUGRA/AS). Underneath each panel, the ratio of the mass function measured from the simulation to the Jenkins et al. mass function is plotted for all models. Note that a logarithmic scale is used on the y-axis in the ratio plots.

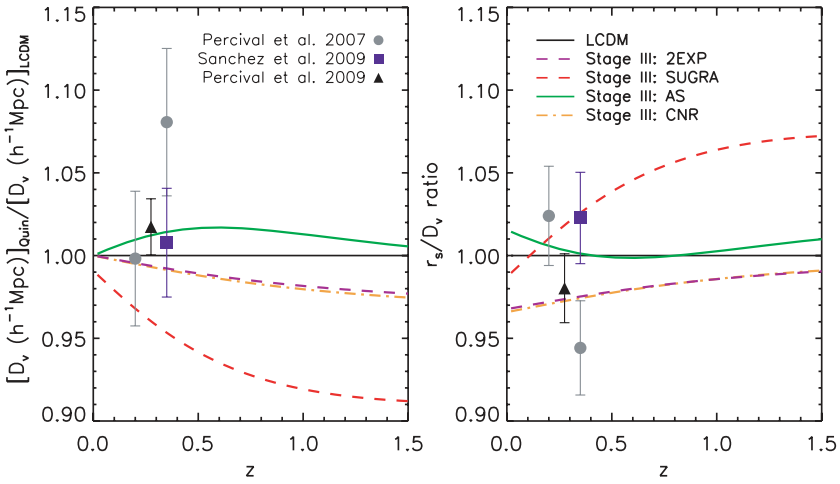

Figure 15. The ratio of the distance measure $D_v(z)$ (left-hand panel) and the ratio of $r_s(z_d)/D_v$ (right-hand panel) for four quintessence models compared to ΛCDM as indicated by the key in the right-hand panel. The grey circles are estimate points from Percival et al. (2007) at $z = 0.2$ and $z = 0.35$ measured using the observed scale of BAO calculated from the SDSS and 2dFGRS main galaxy samples. Sanchez et al. (2009) combined CMB data with information on the shape of the redshift-space correlation function using a larger LRG data set and found $D_v(z = 0.35) = 1300 \pm 31$ Mpc and $r_s(z_d)/D_v = 0.1185 \pm 0.0032$ at $z = 0.35$ (blue squares). The data points from Percival et al. (2009) for D_v and $r_s(z_d)/D_v$ at $z = 0.275$ using *WMAP* 5-yr data + SDSS DR7 are plotted as black triangles.

of D_A and H, given in equation (A6). In most quintessence models, r_s remains unchanged unless there is appreciable dark energy at last scattering. Models which have the same ratio of r_s/D_v are impossible to distinguish using BAO.

To calculate the power spectrum for a galaxy redshift survey, the measured angular and radial separations of galaxy pairs are converted to comoving separations and scales. This conversion is dependent on the cosmological model assumed in the analysis. These changes can be combined into the single effective measure, D_v. Once the power spectrum is calculated in one model, we can simply rescale $P(k)$ using D_v to obtain the power spectrum and BAO peak positions in another cosmological model (see Sanchez et al. 2009). In the left-hand panel of Fig. 15, we plot the ratio of D_v in four quintessence models compared to ΛCDM up to $z = 1.5$. Percival et al. (2007) found $D_v = 564 \pm 23\,h^{-1}$ Mpc at $z = 0.2$ and $D_v = 1019 \pm 42\,h^{-1}$ Mpc at $z = 0.35$ using the observed scale of BAO measured from the Sloan Digital Sky Survey (SDSS) Data Release 5 (DR5) galaxy sample and Two-Degree Field Galaxy Redshift Survey (2dFGRS). These data points are plotted as grey circles in Fig. 15. Note that at face value, none of the models we consider is consistent with the Percival et al. (2007) point at $z = 0.35$. These authors report a 2.4σ discrepancy between their results using BAO and the constraints available at the time from SNe. The blue square plotted in the left-hand panel in Fig. 15 is the constraint $D_v = 1300 \pm 31$ Mpc at $z = 0.35$ found by Sanchez et al. (2009). This constraint was found using a much larger luminous red galaxy (LRG) data set and improved modelling of the correlation function on large scales. The constraint found by Sanchez et al. (2009) using CMB and BAO data is fully consistent with CMB and SN results. The results from Percival et al. (2009) for D_v and $r_s(z_d)/D_v$ at $z = 0.275$ using *WMAP* 5-yr data together with the SDSS DR7 galaxy sample are also plotted (black triangles). The Percival et al. (2009) results are in much better agreement with those of Sanchez et al. (2009).

Over the range of redshifts plotted in Fig. 15 the distance measure, D_v, in the AS, 2EXP and CNR models differs from ΛCDM by at most 2 per cent and is <1 per cent in these models for $z < 0.2$. Rescaling the power spectrum for these dark energy cosmologies would result in a small shift of ∼1 per cent in the position of the peaks at low redshifts. The value of D_v in the SUGRA model differs from ΛCDM by at most 9 per cent up to $z = 1.5$. The right-hand panel in Fig. 15 shows the ratio of $r_s(z_d)/D_v$ in the quintessence models compared to ΛCDM, where r_s is the comoving sound horizon scale at the drag redshift, z_d, which we discuss in Appendix A. The value of $r_s(z_d)/D_v$ can be constrained using the position of the BAO in the power spectrum. In the right-hand panel of Fig. 15, the grey symbols are the results from Percival et al. (2007) at $z = 0.2$ and $z = 0.35$. From this plot, it is clear that the SUGRA and AS models are within the 1σ limits at $z = 0.2$. The 2EXP and CNR models lie just outside the 1σ errors at $z = 0.35$. Note that the value of $r_s(z_d)/D_v$ for ΛCDM at $z = 0.35$ also lies outside the 1σ errors; see Percival et al. (2009) for more detail. The blue square plotted in the right-hand panel in Fig. 15 is $r_s(z_d)/D_v = 0.1185 \pm 0.0032$ at $z = 0.35$ and was obtained using information on the redshift-space correlation function together with CMB data (Sanchez et al. 2009).

In Figs 16 and 17, we plot the $z = 0$ and $z = 3$ power spectra in the AS and SUGRA models divided by a linear theory ΛCDM reference spectrum which has been smoothed using the coarse re-binning method proposed by Percival et al. (2007) and refined by Angulo et al. (2008). After dividing by this smoothed power spectrum, the acoustic peaks are more visible in the quasi-linear regime. In Figs 16 and 17, the measured power in each bin has been multiplied by a factor, f, to remove the scatter due to the small number of large-scale modes in the simulation (Baugh & Efstathiou 1994; Springel et al. 2005). This factor, $f = P(k)_{\mathrm{linear}}/P(k)_{\mathrm{N-body}}$, is the ratio of the expected linear theory power to the measured power in each bin at $z = 5$, at which time the power on these scales is still expected to be linear. Multiplying by this correction factor allows us to see the onset of non-linear growth around $k \sim 0.15\,h\,\mathrm{Mpc}^{-1}$ more clearly.

In Fig. 16 (17), we plot the AS (SUGRA) power spectrum as grey circles from stage I, blue (purple) squares from stage II and green (red) triangles from stage III. The black line represents the linear theory power in ΛCDM divided by the smooth reference spectrum. In both plots and for all power spectra, the same reference spectrum

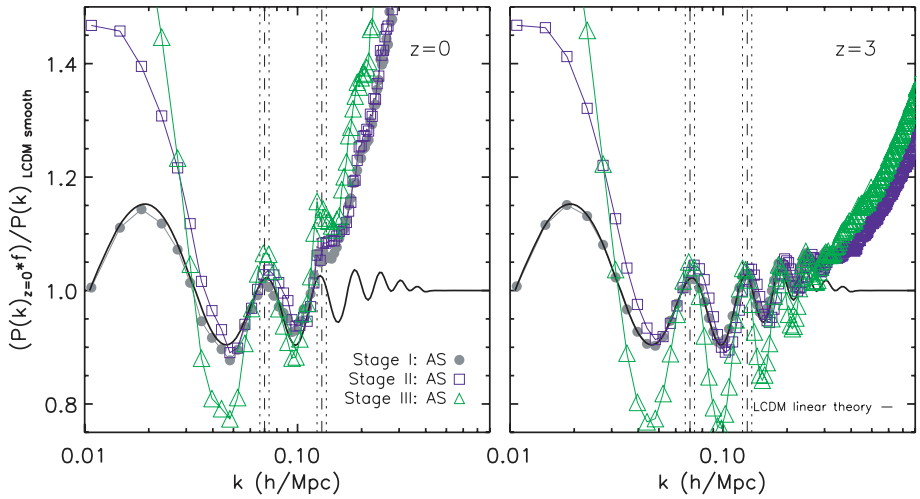

Figure 16. The real space power spectrum for the AS model on large scales at $z = 0$ (left-hand panel) and $z = 3$ (right-hand panel). All power spectra have been divided by a smoothed linear 'no-wiggle' theory $P(k)$ for ΛCDM. The factor, f, removes the scatter of the power measured in the simulation around the expected linear theory power. Stage I in our simulation is represented by grey circles, stage II is represented by open blue squares and stage III results are shown as green triangles. The black solid line represents the linear theory power spectrum in ΛCDM divided by the smooth reference spectrum. The vertical dashed (dotted) lines show the position of the first two acoustic peaks (positions of ± 5 per cent) for a ΛCDM cosmology.

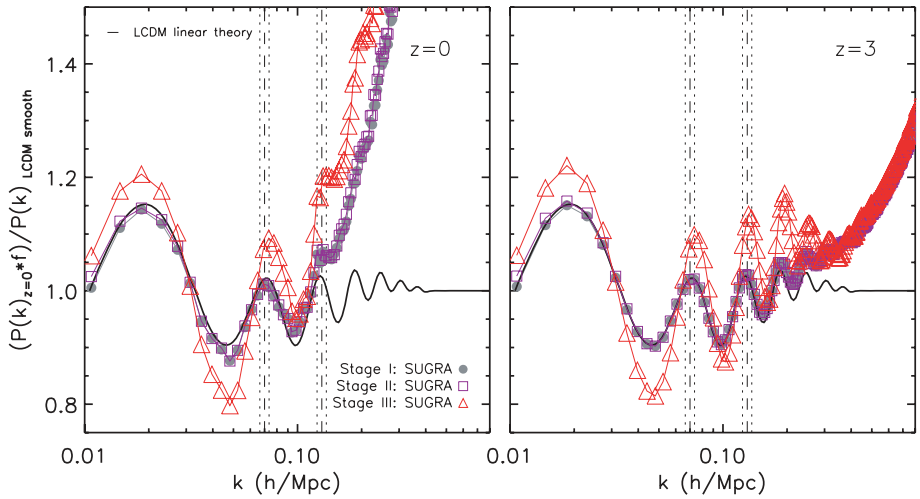

Figure 17. The real space power spectrum for the SUGRA model on large scales at $z = 0$ and $z = 3$. All power spectra have been divided by a smoothed linear theory $P(k)$ for ΛCDM. Stage I in our simulation is represented by grey circles, stage II is represented by open purple squares and stage III results are shown as red triangles. The black solid line represent the linear theory power spectrum in ΛCDM divided by the smooth reference spectrum. The vertical dashed (dotted) lines show the position of the first two acoustic peaks (positions of ±5 per cent) for a ΛCDM cosmology.

is used. The reference is a simple 'wiggle-free' CDM spectrum, with a form controlled by the shape parameter $\Gamma = \Omega_{\rm m} h$ (Bardeen et al. 1986). The difference between the AS and ΛCDM linear theory, as shown in Fig. 11, results in an increase in large-scale power on scales $k < 0.04\,h\,{\rm Mpc}^{-1}$. The vertical dashed (dotted) lines show the first two positions of the acoustic peaks (positions of ± 5 per cent) for a ΛCDM cosmology.

As shown in Fig. 16, we find that the position of the first acoustic peak in the AS model from stage I is the same as in ΛCDM. The position of the first peak for the AS model, measured in stage II of our simulations (blue squares), is slightly shifted (∼4 per cent) to smaller scales compared to ΛCDM as the sound horizon is altered in the AS model. In stage III, when the best-fitting cosmological parameters for the AS model are used, the sound horizon in the AS model and in ΛCDM are very similar at $z \sim 1090$ and there is a very small (<1 per cent) shift in the position of the first peak (green triangles). As there is less non-linear growth at $z = 3$, the higher order peaks are more visible in the right-hand plot in Fig. 16.

In Fig. 17, the SUGRA power spectrum from stages I, II and III is plotted. The SUGRA $P(k)$ from stages I and II have identical peak positions to ΛCDM as the sound horizon is the same as in ΛCDM in these cases. There is a shift (∼5 per cent) in the position of the first peak in the SUGRA model using the $P(k)$ measured in stage III. Note that the units on the x-axis are $h\,{\rm Mpc}^{-1}$ and from Table A3, $h = 0.67$ for the stage III SUGRA model compared to $h = 0.715$ for ΛCDM. On small scales, the BAO signature is damped due to more non-linear structure formation at $z = 0$ compared to $z = 3$ as shown in Fig 17. We find a large increase in the power in the region of the second peak, $k \sim 0.15\,h\,{\rm Mpc}^{-1}$, in both the AS and SUGRA models, measured in stage III, compared to ΛCDM. For brevity, we have not included the plots of the power spectra for the CNR model

showing the BAO. We find identical peak positions in ΛCDM and this model in all stages at $z = 0$.

The AS and SUGRA models are very different to ΛCDM at late times and as result they affect the growth of structure at $z > 0$ as seen in Sections 4.3 and 4.4. We have found that models like this do not necessarily have different BAO peak positions to ΛCDM in the matter power spectrum. These results suggest that distinguishing a quintessence model, such as the AS model used in this paper, using measurements of the BAO peak positions in future galaxy surveys, will be extremely difficult. The BAO peak positions for the CNR model will be shifted by at most 2 per cent in the range $z < 1.5$ compared to ΛCDM after rescaling the power spectra by D_v. In conclusion, it is possible to have quintessence cosmologies with higher levels of dark energy at early times than in ΛCDM and still measure the same peak positions for the BAO in the matter power spectrum.

5 CONCLUSIONS AND SUMMARY

Observing the dynamics of dark energy is the central goal of future galaxy surveys and would distinguish a cosmological constant from a dynamical quintessence model. Using a broad range of quintessence models, with either a slowly or rapidly varying equation of state, we have analysed the influence of dynamical dark energy on structure formation using *N*-body simulations.

We have considered a range of quintessence models that can be classified as either 'tracking' models, for example the SUGRA and INV models, or 'scaling' solutions, such as the AS, CNR or 2EXP model, depending on the evolution of their equation of state (see Table 1 and Section 2.1). The models feature both rapidly and slowly varying equations of state and the majority of the models could be classified as 'early dark energy' models as they have a non-negligible amount of dark energy at early times.

In order to accurately mimic the dynamics of the original quintessence models at high and low redshifts, it is necessary to use a general prescription for the dark energy equation of state which has more parameters than the ubiquitous two-variable equation. Parametrizations for w which use two variables are unable to faithfully represent dynamical dark energy models over a wide range of redshifts and can lead to biases when used to constrain parameters (Bassett et al. 2004). Our task has been made easier by the availability of parametrizations which accurately describe the dynamics of the different quintessence models (Corasaniti & Copeland 2003; Linder & Huterer 2005). This allows us to modify the Friedmann equation in the simulation, using the equation of state as a function of redshift. We use the parametrization of Corasaniti & Copeland (2003). In its full six-parameter form, this framework can describe the quintessence model back to the epoch of nucleosynthesis. Four parameters are sufficient to describe the behaviour of the quintessence field over the redshift interval followed by the simulations. With this description of the equation of state, our simulations are able to accurately describe the impact of the quintessence model on the expansion rate of the Universe, from the starting redshift to the present day. This would not be the case with a two-parameter model for the equation of state.

In this paper, we have taken into account three levels of modification from a ΛCDM cosmology which are necessary if we wish to faithfully incorporate the effects of quintessence dark energy into a *N*-body simulation. The first stage is to replace the cosmological constant with the quintessence model in the Friedmann equation. A quintessence model with a different equation of state from $w = -1$ will lead to a universe with a different expansion history. This in turn alters the rate at which perturbations can collapse under gravity. The second stage is to allow the change in the expansion history and perturbations in the quintessence field to have an impact on the form of the linear theory power spectrum. The shape of the power spectrum can differ significantly from ΛCDM on large scales if there is a non-negligible amount of dark energy present at early times. This alters the shape of the turnover in the power spectrum compared to ΛCDM. Thirdly, as the quintessence model should be consistent with observational constraints, the cosmological parameters used for the dark energy model could be different from the best-fitting ΛCDM parameters. In the three stages of simulations, we look at the effect each of the above modifications has on the non-linear growth of structure. Deconstructing the simulations into three stages allows us to isolate specific features in the quintessence models which play a key role in the growth of dark matter perturbations.

In the first stage of comparison, in which all that is changed is the expansion history of the universe, we found that some of the quintessence models showed enhanced structure formation at $z > 0$ compared to ΛCDM. The INV1, INV2, SUGRA and AS models have slower growth rates than ΛCDM. Hence, when normalizing to the same σ_8 today, structures must form at earlier times in these models to overcome the lack of growth at late times. Models such as 2EXP and CNR have the same recent growth rate as ΛCDM and showed no difference in the growth of structure. The difference in linear and non-linear growth can largely be explained by the difference in the growth factor at different epochs in the models. At the same growth factor, the power in the models only diverges at the 15 per cent level well into the non-linear regime.

In the second stage, a self-consistent linear theory $P(k)$ was used for each quintessence model to generate the initial conditions in the simulations. The amount of dark energy present at early times will determine the impact on the linear theory dark matter power spectrum and the magnitude of deviation from the ΛCDM spectrum. High levels of dark energy at early times suppress the growth of the dark matter on scales inside the horizon, resulting in a broader turnover in the power spectrum. We found that models with the highest levels of dark energy at the last scattering surface, such as the AS and CNR models, have linear theory $P(k)$ which differs the most from ΛCDM. The results of the *N*-body simulations of the AS and SUGRA models show a very small increase in non-linear growth compared to the results in stage I. The increase in the linear theory power is on very large scales and does not change the small-scale growth significantly.

In our final stage of simulating the effects of quintessence, we found the best-fitting cosmological parameters for each model, $\Omega_m h^2$, $\Omega_b h^2$ and H_0, consistent with the current CMB, SN and BAO measurements. For quintessence dark energy models, it is important to consider the changes in more than just one cosmological parameter when fitting to the observational data. For example, for a given dark energy equation of state, the values of $\Omega_m h^2$ and H_0 may change in such a way to compensate one another and give similar growth rates and expansion histories to ΛCDM. These compensating effects will be missed if, for example, only Ω_m is changed for the dark energy model as in recent work (Alimi et al. 2009). Models with cosmological parameters which fit the data but were significantly different from ΛCDM were simulated again (Section 4.3).

We will now summarize and discuss the main results for each model. The key features of each of the quintessence models are presented in Table 2. The INV1 model was unable to fit the data with a reasonable χ^2/ν (Table A3). This toy model had the largest growth factor ratio to ΛCDM at $z = 5$ and as a result showed the most enhanced growth in stage I of our simulations. The linear growth factor for the INV2 model is very different to ΛCDM at

Table 2. The key features in the evolution of the quintessence models simulated. $\Delta D(z = 5)$ is the ratio of the linear growth factor for each quintessence model compared to ΛCDM at $z = 5$. A late-time transition in the equation of state is defined as occurring at $z < 2$. The AS, CNR, 2EXP and SUGRA models can be considered as 'early dark energy ' models as they have non-negligible amounts of dark energy present at early times.

Model	Transition type	Transition redshift	$\Omega_{\rm DE}(z = 300)$	$\Delta D\ (z = 5)$
INV1	Gradual	∼4.5	∼0.009	∼50 per cent
INV2	Gradual	∼5	Negligible	∼10 per cent
SUGRA	Rapid	∼9	∼0.01	∼20 per cent
2EXP	Rapid	∼4	∼0.015	0 per cent
CNR	Rapid	∼5.5	∼0.03	0 per cent
AS	Rapid	∼1	∼0.11	20 per cent

early times and gives rise to enhanced growth at $z > 0$ as seen in Section 4.1. This model has negligible dark energy at early times and so the spectral shape is not altered in stage II. In the 2EXP model the rapid transition to $w = -1$ in the equation of state early on leaves little impact on the growth of dark matter, and as a result the power spectra and mass function are indistinguishable from ΛCDM. As both the INV2 and 2EXP models already agree with cosmological measurements with very similar values for $\Omega_{\rm m}h^2$, $\Omega_{\rm b}h^2$ and H_0 to ΛCDM, we did not run these simulations again.

The SUGRA model has enhanced linear and non-linear growth and halo abundances compared to ΛCDM at $z > 0$ and an altered linear theory power spectrum shape. The mass function results for all stages of our simulations for the SUGRA model show enhanced halo abundances at $z > 0$. Analysing the SUGRA power spectra, from a stage III simulation which used the best-fitting parameters for this model, reveals an ∼5 per cent shift in the position of the first BAO peak. We find that the distance measure D_v for the SUGRA model differs by up to 9 per cent compared to ΛCDM over the range $0 < z < 1.5$. Rescaling the power measured for the SUGRA model by the difference in D_v would result in an even larger shift in the position of the BAO peaks.

The CNR model has high levels of dark energy early on which alters the spectral shape on such large scales that the non-linear growth of structure is only slightly less than ΛCDM at $z < 5$. This model has a halo mass abundance at $z < 5$ and BAO peak positions at $z = 0$ which are the same as in ΛCDM. For $z < 0.5$ the distance measure, D_v, for the CNR model differs from ΛCDM by ∼1 per cent; as a result, there would be a corresponding small shift in the BAO peak positions. The rapid early transition at $z = 5.5$ in the equation of state to $w_0 = -1$ in this model seems to remove any signal of the large amounts of dark energy at early times that might be present in the growth of dark matter perturbations.

The AS model has the highest levels of dark energy at early times, and so its linear theory spectrum is altered the most. This results in a large increase in large-scale power, when we normalize the power spectrum to $\sigma_8 = 0.8$ today. The results from stage III using the best-fitting parameters show both enhanced linear and non-linear growth at $z < 5$. The linear theory $P(k)$ is altered on scales $k \sim 0.1\,h\,{\rm Mpc}^{-1}$ which drives an increase in non-linear growth on small scales compared to ΛCDM. The mass function results in stage III for this model show enhanced halo abundances at $z > 0$. We find that using the best-fitting cosmological parameters for the AS model produces a BAO profile with peak positions similar to those in ΛCDM. At low redshifts there is an ∼1 per cent shift in the first peak compared to ΛCDM after rescaling the power with the difference in the distance measure D_v between the two cosmologies.

These results from stage III of our N-body simulations show that dynamical dark energy models in which the dark energy equation of state makes a late ($z < 2$) rapid transition to $w_0 = -1$ show enhanced linear and non-linear growth compared to ΛCDM at $z > 0$ and have a greater abundance of dark matter haloes compared to ΛCDM for $z > 0$. We found that dynamical dark energy models can be significantly different from ΛCDM at late times and still produce similar BAO peak positions in the matter power spectrum. Models which have a rapid early transition in their dark energy equation of state and mimic ΛCDM after the transition show the same linear and non-linear growth and halo abundance as ΛCDM for all redshifts. We have found that these models can give rise to BAO peak positions in the matter power spectrum which are the same as those in a ΛCDM cosmology. This is true despite these models having non-negligible amounts of dark energy present at early times.

Overall, our analysis shows that the prospects of detecting dynamical dark energy, which features a late-time transition, using the halo mass function at $z > 0$ are good, provided a good proxy can be found for mass. Parameter degeneracies allow some quintessence models to have identical BAO peak positions to ΛCDM and so these measurements alone will not be able to rule out some quintessence models. Although including the dark energy perturbations has been found to increase these degeneracies (Weller & Lewis 2003), incorporating them into the N-body code would clearly be the next step towards simulating quintessential dark matter with a full physical model. Although in many quintessence models the dark energy clusters on very large scales today ($k < 0.02\,h\,{\rm Mpc}^{-1}$) (Weller & Lewis 2003) and the perturbations are generally small ($\delta_{\rm DE} \sim 10^{-1}$), these perturbations may nevertheless have some impact on the dark matter structure in a full N-body simulation of the non-linear growth.

ACKNOWLEDGMENTS

EJ acknowledges receipt of a fellowship funded by the European Commission's Framework Programme 6, through the Marie Curie Early Stage Training project MEST-CT-2005-021074. This work was supported in part by grants from the Science and Technology Facilities Council held by the Extragalactic Cosmology Research Group and the Institute for Particle Physics Phenomenology at Durham University. We acknowledge helpful conversations with Simon D. M. White, Ariel G. Sánchez, Shaun Cole and Lydia Heck for support in running the simulations.

REFERENCES

Albrecht A. J., Skordis C., 2000, Phys. Rev. Lett., 84, 2076
Alimi J., Fuzfa A., Boucher V., Rasera Y., Courtin J., Corasaniti P., 2009, preprint (arXiv:0903.5490)
Angulo R., Baugh C. M., Frenk C. S., Lacey C. G., 2008, MNRAS, 383, 755
Bardeen J. M., Bond J. R., Kaiser N., Szalay A. S., 1986, ApJ, 304, 15

Barreiro T., Copeland E. J., Nunes N. J., 2000, Phys. Rev. D, 61, 127301
Bassett B. A., Kunz M., Silk J., Ungarelli C., 2002, MNRAS, 336, 1217
Bassett B. A., Corasaniti P. S., Kunz M., 2004, ApJ, 617, L1
Baugh C. M., Efstathiou G., 1994, MNRAS, 270, 183
Baugh C. M., Gaztanaga E., Efstathiou G., 1995, MNRAS, 274, 1049
Baumgart D. J., Fry J. N., 1991, ApJ, 375, 25
Bean R., Hansen S. H., Melchiorri A., 2001, Phys. Rev. D, 64, 103508
Bond J. R., Efstathiou G., Tegmark M., 1997, MNRAS, 291, L33
Brax P., Martin J., 1999, Phys. Lett. B, 468, 40
Caldwell R. R., Dave R., Steinhardt P. J., 1998, Phys. Rev. Lett., 80, 1582
Caldwell R. R., Doran M., Mueller C. M., Schafer G., Wetterich C., 2003, ApJ, 591, L75
Carroll S. M., 2001, Living Rev. Rel., 4, 1
Casarini L., Macciò A. V., Bonometto S. A., 2009, J. Cosmology Astropart. Phys., 3, 14
Chevallier M., Polarski D., 2001, Int. J. Mod. Phys. D, 10, 213
Copeland E. J., Nunes N. J., Rosati F., 2000, Phys. Rev. D, 62, 123503
Copeland E. J., Sami M., Tsujikawa S., 2006, Int. J. Mod. Phys. D, 15, 1753
Corasaniti P. S., 2004, PhD thesis, Univ. Sussex (astro-ph/0401517)
Corasaniti P. S., Copeland E. J., 2003, Phys. Rev. D, 67, 063521
Corasaniti P. S., Kunz M., Parkinson D., Copeland E. J., Bassett B. A., 2004, Phys. Rev. D, 70, 083006
Crocce M., Fosalba P., Castander F. J., Gaztanaga E., 2009, preprint (arXiv:0907.0019)
Doran M., Robbers G., 2006, J. Cosmology Astropart. Phys., 0606, 026
Doran M., Robbers G., Wetterich C., 2007, Phys. Rev. D, 75, 023003
Efstathiou G., Rees M. J., 1988, MNRAS, 230, 5
Eisenstein D. J., Hu W., 1998, ApJ, 496, 605
Eisenstein D. J. et al., 2005, ApJ, 633, 560
Eke V. R., Cole S., Frenk C. S., 1996, MNRAS, 282, 263
Eke V. R., Navarro J. F., Steinmetz M., 2001, ApJ, 554, 114
Fang W., Hu W., Lewis A., 2008, Phys. Rev. D, 78, 087303
Ferreira P. G., Joyce M., 1998, Phys. Rev. D, 58, 023503
Francis M. J., Lewis G. F., Linder E. V., 2008, MNRAS, 394, 605
Gaztanaga E., Cabre A., Hui L., 2008, preprint (arXiv:0807.3551)
Gerke B. F., Efstathiou G., 2002, MNRAS, 335, 33
Governato F. et al., 1999, MNRAS, 307, 949
Grossi M., Springel V., 2009, MNRAS, 394, 1559
Guy J., Astier P., Nobili S., Regnault N., Pain R., 2005, A&A, 443, 781
Halliwell J. J., 1987, Phys. Lett. B, 185, 341
Hockney R. W., Eastwood J. W., 1981, Computer Simulation Using Particles. McGraw-Hill Inc., New York
Hu W., Sugiyama N., 1996, ApJ, 471, 542
Jenkins A., Frenk C. S., White S. D. M., Colberg J. M., Cole S., Evrard A. E., Couchman H. M. P., Yoshida N., 2001, MNRAS, 321, 372
Klypin A., Maccio A. V., Mainini R., Bonometto S. A., 2003, ApJ, 599, 31
Komatsu E. et al., 2009, ApJS, 180, 330
Kowalski M. et al., 2008, ApJ, 686, 749
Kunz M., Corasaniti P.-S., Parkinson D., Copeland E. J., 2004, Phys. Rev. D, 70, 041301
Lacey C. G., Cole S., 1994, MNRAS, 271, 676
Lewis A., Bridle S., 2002, Phys. Rev. D, 66, 103511
Li H., Xia J.-Q., Zhao G.-B., Fan Z.-H., Zhang X., 2008, ApJ, 683, L1
Linder E. V., 2003, Phys. Rev. Lett., 90, 091301
Linder E. V., 2008, Gen. Relativ. Grav., 40, 329
Linder E. V., Huterer D., 2005, Phys. Rev. D, 72, 043509
Linder E. V., Jenkins A., 2003, MNRAS, 346, 573
Ma C.-P., Caldwell R. R., Bode P., Wang L.-M., 1999, ApJ, 521, L1
Percival W. J. et al., 2007, MNRAS, 381, 1053
Percival W. J. et al., 2009, preprint (arXiv:0907.1660)
Press W. H., Schechter P., 1974, ApJ, 187, 425 (P-S)
Ratra B., Peebles P. J. E., 1988, Phys. Rev. D, 37, 3406
Reed D., Bower R., Frenk C., Jenkins A., Theuns T., 2007, MNRAS, 374, 2
Sanchez A. G., Baugh C. M., Angulo R., 2008, MNRAS, 390, 1470
Sanchez A. G., Crocce M., Cabre A., Baugh C. M., Gaztanaga E., 2009, preprint (arXiv:0901.2570)
Sheth R. K., Tormen G., 2002, MNRAS, 329, 61 (S-T)
Sheth R. K., Mo H. J., Tormen G., 2001, MNRAS, 323, 1
Smith R. E. et al., 2003, MNRAS, 341, 1311
Springel V., 2005, MNRAS, 364, 1105
Springel V. et al., 2005, Nat, 435, 629
Steinhardt P. J., Wang L.-M., Zlatev I., 1999, Phys. Rev. D, 59, 123504
Wands D., Copeland E. J., Liddle A. R., 1993, Ann. NY Acad. Sci., 688, 647
Warren M. S., Abazajian K., Holz D. E., Teodoro L., 2006, ApJ, 646, 881
Weller J., Lewis A. M., 2003, MNRAS, 346, 987
Wetterich C., 1988, Nucl. Phys. B, 302, 668
Wetterich C., 1995, A&A, 301, 321
Wetterich C., 2004, Phys. Lett. B, 594, 17
White S. D. M., 1994, RvMA, 7, 255
White S. D. M., Efstathiou G., Frenk C. S., 1993, MNRAS, 262, 1023
Xia J.-Q., Viel M., 2009, J. Cosmology Astropart. Phys., 0904, 002
Zlatev I., Wang L.-M., Steinhardt P. J., 1999, Phys. Rev. Lett., 82, 896

APPENDIX A: OBSERVATIONAL DISTANCE PRIORS

In this section, we outline the method used to find the best-fitting cosmological parameters for each of the quintessence models using CMB, BAO and SN data. The method suggested in Komatsu et al. (2009) employs three distance priors from measurements of the CMB together with the 'UNION' SN samples (Kowalski et al. 2008) and the BAO in the distribution of galaxies (Percival et al. 2007) to explore the best-fitting parameters for the dynamical dark energy models. In Sections 4.1 and 4.2, all of the quintessence simulations were run using the best-fitting cosmological parameters assuming a ΛCDM model. While this is useful for isolating the effect of the different expansion histories on the growth of structure, this does not yield quintessence models which would automatically satisfy the constraints on distance measurements. Using CMB, SNe and BAO data in this way is very useful for testing and perhaps even ruling out some of the dark energy quintessence models. In Section 4.3, we consider the impact of using these new cosmological parameters on the non-linear growth of structure.

These distance priors are derived parameters which depend on the assumed cosmological model and yield constraints on dark energy parameters which are slightly weaker than a full Markov Chain Monte Carlo (MCMC) calculation, as only part of the full *WMAP* data is used, i.e. the C_l spectrum is condensed into two or three numbers describing peak position and ratios and the polarization data are ignored. The assumed model is a standard FLRW universe with an effective number of neutrinos equal to 3.04 and a nearly power-law primordial power spectrum with negligible primordial gravity waves and entropy fluctuations. These *WMAP* distance priors are extremely useful for providing cosmological parameter constraints at a reduced computational cost compared to a full MCMC calculation.

We shall briefly review the distance scales used in this paper and the method for finding the best-fitting parameters for the dark energy models. From measurements of the peaks and troughs of the acoustic oscillations in the photon–baryon plasma in the CMB, it is possible to measure two distance ratios (Komatsu et al. 2009). The first ratio is quantified by the 'acoustic scale', $l_{\rm A}$, which is defined in terms of the sound horizon at decoupling, $r_{\rm s}(z_*)$, and the angular diameter distance to the last scattering surface, $D_{\rm A}(z_*)$, as

$$l_{\rm A} = (1+z_*)\frac{\pi D_{\rm A}(z_*)}{r_{\rm s}(z_*)}. \tag{A1}$$

Assuming a flat universe, the proper angular diameter distance is defined as

$$D_{\rm A}(z) = \frac{c}{(1+z)}\int_0^z \frac{{\rm d}z'}{H(z')}, \tag{A2}$$

and the comoving sound horizon is given by

$$r_s(z) = \frac{c}{\sqrt{3}} \int_0^{1/(1+z)} \frac{da}{a^2 H(a)\sqrt{1+(3\Omega_b/4\Omega_\gamma)a}}, \quad \text{(A3)}$$

where $\Omega_\gamma = 2.469 \times 10^{-5} h^{-2}$ for $T_{CMB} = 2.725$ K (Komatsu et al. 2009) and Ω_b is the ratio of the baryon energy density to the critical density. We shall use the fitting formula proposed by Hu & Sugiyama (1996) for the decoupling epoch z_* which is a function of $\Omega_b h^2$ and $\Omega_m h^2$ only. The second distance ratio measured by the CMB is called the 'shift parameter' (Bond, Efstathiou & Tegmark 1997). This is the ratio of the angular diameter distance to the Hubble horizon size at the decoupling epoch which is written as

$$R(z_*) = \frac{\sqrt{\Omega_m H_0^2}}{c}(1+z_*)D_A(z_*). \quad \text{(A4)}$$

Equation (A4) assumes a standard radiation- and matter-dominated epoch when calculating the sound horizon. The expression for the shift parameter will be modified for quintessence models of dark energy. The proper expression for the shift parameter is given by (Kowalski et al. 2008)

$$R(z_*) = R_{std}(z_*)\left(\int_{z_*}^{\infty} \frac{dz/\sqrt{\Omega_m(1+z)^3}}{\int_{z_*}^{\infty} dz H_0/H(z)}\right), \quad \text{(A5)}$$

where R_{std} is the standard shift parameter given in equation (A4). This correction to the shift parameter can be substantial for quintessence models with non-negligible amounts of dark energy at early times and so we include this correction for all of the scalar field models in this paper. The 5-yr *WMAP* constraints on l_A, R and the redshift at decoupling z_* are the *WMAP* distance priors used to test models of dark energy (Komatsu et al. 2009).

The angular diameter distance at the decoupling epoch can be determined from measurements of the acoustic oscillations in the CMB. These BAO are also imprinted on the distribution of matter. Using galaxies as tracers for the underlying matter distribution, the clustering perpendicular to the line of sight gives a measurement of the angular diameter distance, $D_A(z)$. BAO data also allow us to measure the expansion rate of the universe, $H(z)$, from observations of clustering along the line of sight. Recently, Gaztanaga, Cabre & Hui (2008) made a direct measurement of the Hubble parameter as a function of redshift providing for the first time a measure of $D_A(z)$ and $H(z)$ individually. Using a spherically averaged correlation function to reveal the BAO signal results in an effective distance measure given by (Eisenstein et al. 2005)

$$D_V(z) = \left((1+z)^2 D_A^2(z)\frac{cz}{H(z)}\right)^{1/3}. \quad \text{(A6)}$$

It is the ratio of $D_V(z)$ to the sound horizon, r_s, at the drag epoch, z_{drag}, which determines the peak positions of the BAO signal. The drag epoch is the redshift at which baryons are separated from photons and is slightly later than the decoupling epoch, z_*. For a wide angle survey, D_v is used, which is motivated on dimensional grounds and equal sampling of all axes (e.g. D_v for a pencil beam survey would have different exponents of D_A and H). Percival et al. (2007) provide $r_s(z_d)/D_V(z)$ at two redshifts, $z = 0.2$ and $z = 0.35$, taken from the SDSS and 2dFGRS. The two values are $r_s(z_d)/D_V(0.2) = 0.198 \pm 0.0058$ and $r_s(z_d)/D_V(0.35) = 0.1094 \pm 0.0033$, respectively.

The UNION SNe compilation (Kowalski et al. 2008) consists of 307 low-redshift SN all processed using the SALT light-curve fitter (Guy et al. 2005). This compilation includes older data sets from the Supernova Legacy Survey and ESSENCE Survey as well as a recent data set observed with the *Hubble Space Telescope* (*HST*). Type Ia SNe data are extremely useful in breaking parameter degeneracies such as the w, Ω_{DE} degeneracy in the CMB data. A wide range of these two parameters can produce similar angular diameter distances at the redshift of decoupling and so SN constraints, which are almost orthogonal to CMB constraints, help to reduce this parameter space. The current SN data cover a wide range of redshifts, $0.02 \leq z \leq 1.7$, but is only able to weakly constrain a dynamical dark energy equation of state, w, at $z \geq 1$. Also, due to a degeneracy with Ω_m, the current SN data by themselves are not able to tightly constrain the present value of w and including measurements involving Ω_m such as CMB or BAO observations breaks this degeneracy.

Following the prescription of Komatsu et al. (2009) for using the *WMAP* distance priors, it is necessary to find the vector $\boldsymbol{x} = (l_A, R, z_*)$ for each quintessence model in order to compute the likelihood, $\mathcal{L}$, as $\chi^2 = -2\ln\mathcal{L} = (x_i - d_i)C_{ij}^{-1}(x_j - d_j)$, where $\boldsymbol{d} = (l_A^{WMAP}, R^{WMAP}, z_*^{WMAP})$ and C_{ij}^{-1} is the inverse covariance matrix for the *WMAP* distance priors.

In order to find the best-fitting cosmological parameters for each quintessence model, we minimize the function $\chi^2_{total} = \chi^2_{WMAP} + \chi^2_{BAO} + \chi^2_{SN}$ with respect to $\Omega_m h^2$, $\Omega_b h^2$ and H_0. In appendix D of Komatsu et al. (2009), it can be seen that including the systematic errors has a very small effect on the ΛCDM parameters but can have a significant impact on dark energy parameters. Using a two-parameter equation of state for the dark energy, Komatsu et al. (2009) found that the parameter constraints weakened considerably after including systematic errors. In calculating χ^2_{SN} in this paper, we have used the covariance matrix for the errors on the SN distance moduli without systematic errors.

Table A1 shows the *WMAP* distance priors computed for each dark energy model using the cosmological parameters from Sanchez

Table A1. Distance priors based on *WMAP* observations (Komatsu et al. 2009) for each quintessence model using $\Omega_m h^2$, $\Omega_b h^2$ and H_0 parameters from Sanchez et al. (2009). These parameters were derived assuming a ΛCDM cosmology. $l_A(z_*)$ is the acoustic scale at the epoch of decoupling, z_*, and $R(z_*)$ is the shift parameter. $\chi^2_{total} = \chi^2_{WMAP+SN+BAO}$ and ν is the number of degrees of freedom.

	$z*$	$l_A(z*)$	$R(z*)$	χ^2_{total}/ν
WMAP 5-yr ML	1090.51 ± 0.95	302.10 ± 0.86	1.710 ± 0.019	0
INV1	–	261.05	1.49	15.34
INV2	–	294.34	1.67	1.81
SUGRA	–	284.03	1.62	3.88
2EXP	–	303.85	1.74	1.09
AS	–	289.69	1.74	2.04
CNR	–	306.71	1.79	1.37

Table A2. BAO distance measurements (Percival et al. 2007) for each quintessence model using $\Omega_m h^2$, $\Omega_b h^2$ and H_0 parameters from Sanchez et al. (2009). These parameters were derived assuming a ΛCDM cosmology. A fitting formula proposed by Eisenstein & Hu (1998) was used for the drag redshift z_{drag}.

	z_{drag}	$r_s(z_{drag})$	$r_s(z_{drag})/D_v(z=0.2)$	$r_s(z_{drag})/D_v(z=0.2)$
WMAP 5-yr	1020.5 ± 1.6	153.3 ± 2.0 Mpc	-	-
Percival et al. (2007)	–	154.758 Mpc	0.198 ± 0.0058	0.1094 ± 0.0033
INV1	–	152.5 Mpc	0.208	0.130
INV2	–	152.7 Mpc	0.198	0.121
SUGRA	–	152.5 Mpc	0.198	0.121
2EXP	–	152.0 Mpc	0.192	0.115
AS	–	143.9 Mpc	0.183	0.111
CNR	–	150.7 Mpc	0.191	0.114

Table A3. Best-fitting values for $\Omega_m h^2$, $\Omega_b h^2$ and H_0 with 68.3 per cent confidence intervals by minimizing $\chi^2_{total} = \chi^2_{WMAP+SN+BAO}$ for each quintessence model. wCDM *WMAP* 5 yr are the parameter constraints assuming a dynamical dark energy model (Komatsu et al. 2009).

	$10^2\Omega_b h^2$	H_0 (km s^{-1} Mpc^{-1})	$\Omega_m h^2$	χ^2_{total}/ν
ΛCDM *WMAP* 5-yr mean	$2.267^{+0.058}_{-0.059}$	70.5 ± 1.3	$0.1358^{+0.0037}_{-0.0036}$	
wCDM *WMAP* 5-yr mean	2.27 ± 0.06	69.7 ± 1.4	0.1351 ± 0.0051	
Sanchez et al. (2009)	$2.267^{+0.049}_{-0.05}$	71.5 ± 1.1	0.13343 ± 0.0026	1.09
INV1	3.78 ± 0.145	63.13 ± 0.5	0.115 ± 0.0103	2.27
INV2	2.35 ± 0.094	68.21 ± 0.7	0.124 ± 0.0065	1.07
SUGRA	2.68 ± 0.105	67.63 ± 0.7	0.111 ± 0.0075	1.25
2EXP	2.22 ± 0.115	70.01 ± 0.8	0.138 ± 0.0031	1.05
AS	2.12 ± 0.121	70.42 ± 0.9	0.086 ± 0.0121	1.07
CNR	2.09 ± 0.185	70.05 ± 1.2	0.140 ± 0.0133	1.12

et al. (2009). The BAO scale and drag redshift, z_d, are given in Table A2 using the same parameters. From these tables, it is clear that some quintessence models with ΛCDM cosmological parameters fail to agree with the distance measurements within the current constraints.

With the assumption that $\Omega_m h^2$, $\Omega_b h^2$ and H_0 are tightly constrained by *WMAP*, BAO and SN data, and as a result their posterior distribution is close to a normal distribution, minimizing $\chi^2_{total} = \chi^2_{WMAP} + \chi^2_{BAO} + \chi^2_{SN}$ with respect to these three parameters will be the same as marginalizing the posterior distribution. We have fixed the dark energy equation-of-state parameters for each quintessence model, and the 68.3 per cent confidence intervals for each parameter by minimizing χ^2_{total} are shown in Table A3. The final column in this table is χ^2/ν, where ν is the number of degrees of freedom. From Table A3, it is clear that the INV1 model is unable to fit the data and has a poor $\chi^2/\nu = 2.27$ statistic. Most of the quintessence models favour a lower $\Omega_m h^2$ compared to ΛCDM in order to fit the distance data. As can be seen from Table A3, the confidence intervals on the three fitted parameters $\Omega_m h^2$, $\Omega_b h^2$ and H_0 are quite large. Once the best-fitting parameters from Table A3 are used, all of the quintessence models apart from INV1 which we rule out produce a better fit to the data, as seen in Tables A4 and A5, for the *WMAP* distance priors and the BAO distance measures, respectively. As we noted earlier, the *WMAP* distance priors do not contain all of the *WMAP* power spectrum data and only use the information from the oscillations present at small angular scale (high multipole moments). Neglecting the Sachs–Wolfe (SW) effect at large angular scales (small multipole moments) as well as polarization data leads to weaker constraints on cosmological parameters in these dark energy models. We have not considered how these distance priors would change with the inclusion of dark energy perturbations (Li et al. 2008). These results are in agreement with previous work fitting cosmological parameters of quintessence models using *WMAP* first-year CMB data and SN data (Corasaniti et al. 2004).

Table A4. *WMAP* distance priors (Komatsu et al. 2009) for each quintessence model using the best-fitting parameters $\Omega_m h^2$, $\Omega_b h^2$ and H_0 given in Table A3.

	$z*$	$l_A(z*)$	$R(z*)$
ΛCDM *WMAP* 5-yr ML	1090.51 ± 0.95	302.10 ± 0.86	1.710 ± 0.019
Sanchez et al. 2009	1090.12 ± 0.93	301.58 ± 0.67	1.701 ± 0.018
INV1	1076.17	292.54	1.519
INV2	1088.71	301.69	1.676
SUGRA	1083.96	298.51	1.596
2EXP	1091.75	302.91	1.749
AS	1087.98	300.23	1.684
CNR	1093.97	303.51	1.809

Table A5. BAO distance measurements (Percival et al. 2007) for each quintessence model using the best-fitting parameters $\Omega_m h^2$, $\Omega_b h^2$ and H_0 given in Table A3.

	z_{drag}	$r_s(z_{drag})$	$r_s/D_V(z=0.2)$	$r_s/D_V(z=0.35)$
WMAP 5-yr	1020.5 ± 1.6	153.3 ± 2.0 Mpc	–	–
Percival et al. (2007)	–	154.758 Mpc	0.198 ± 0.0058	0.1094 ± 0.0033
INV1	1045.1	146.259 Mpc	0.1765	0.1103
INV2	1021.2	154.946 Mpc	0.1921	0.1167
SUGRA	1026.4	155.803 Mpc	0.1908	0.1161
2EXP	1019.9	150.983 Mpc	0.1879	0.1123
AS	1010.5	157.745 Mpc	0.1947	0.1161
CNR	1017.1	150.597 Mpc	0.1876	0.1128

This paper has been typeset from a TEX/LATEX file prepared by the author.